Cell Chem Biol. 2018 Dec 20; 25(12): 1456–1469.e6.

doi: 10.1016/j.chembiol.2018.09.005: 10.1016/j.chembiol.2018.09.005

PMCID: PMC6309505

NIHMSID: NIHMS993720

PMID: 30293938

ALDH1 Bio-activates Nifuroxazide to Eradicate ALDH^{High} Melanoma-Initiating Cells

Sana Sarvi,[1,2,12] Richard Crispin,[2,12] Yuting Lu,[1,2] Lifan Zeng,[3] Thomas D. Hurley,[3] Douglas R. Houston,[4] Alex von Kriegsheim,[2] Che-Hong Chen,[5] Daria Mochly-Rosen,[5] Marco Ranzani,[6,7] Marie E. Mathers,[8] Xiaowei Xu,[9] Wei Xu,[10] David J. Adams,[6] Neil O. Carragher,[2] Mayumi Fujita,[11] Lynn Schuchter,[10] Asier Unciti-Broceta,[2] Valerie G. Brunton,[2] and E. Elizabeth Patton[1,2,13,*]

[1]MRC Human Genetics Unit, MRC Institute of Genetics and Molecular Medicine, University of Edinburgh, Edinburgh EH4 2XR, UK

[2]Cancer Research UK Edinburgh Centre, MRC Institute of Genetics and Molecular Medicine, University of Edinburgh, Edinburgh EH4 2XR, UK

[3]Department of Biochemistry & Molecular Biology, Indiana University School of Medicine, 635 Barnhill Drive Medical Science, Indianapolis, IN 46202, USA

[4]School of Biological Sciences, University of Edinburgh, Waddington Building, King's Buildings, Max Born Crescent, Edinburgh EH9 3BF, UK

[5]Department of Chemical and Systems Biology, Stanford University School of Medicine, 269 Campus Drive, Stanford, CA 94305-5174, USA

[6]Experimental Cancer Genetics, Wellcome Trust Sanger Institute, Hinxton, Cambridge CB10 1HH, UK

[7]Biology Team, Artios Pharma Limited, Meditrina (B 260), Babraham Research Campus, Cambridge CB22 3AT, UK

[8]Department of Pathology, Western General Hospital, Crewe Road, Edinburgh EH4 2XU, UK

[9]Department of Pathology and Laboratory Medicine, University of Pennsylvania, Philadelphia, PA 19104, USA

[10]Abramson Cancer Center University of Pennsylvania, Philadelphia, PA 19104, USA

[11]Department of Dermatology, University of Colorado Anschutz Medical Campus, 12801 E 17th Avenue, RC-1S, Aurora, CO 80045, USA

E. Elizabeth Patton: e.patton@igmm.ed.ac.uk

*Corresponding author e.patton@igmm.ed.ac.uk

[12]These authors contributed equally

[13]Lead Contact

Received 2018 Jan 30; Revised 2018 Jun 25; Accepted 2018 Sep 7.

Summary

5-Nitrofurans are antibiotic pro-drugs that have potential as cancer therapeutics. Here, we show that 5-nitrofurans can be bio-activated by aldehyde dehydrogenase (ALDH) 1A1/1A3 enzymes that are highly expressed in a subpopulation of cancer-initiating (stem) cells. We discover that the 5-nitrofuran, nifuroxazide, is selective for bio-activation by ALDH1 isoforms over ALDH2, whereby it both oxidizes ALDH1 and is converted to cytotoxic metabolites in a two-hit pro-drug mechanism. We show that ALDH1^{High} melanoma cells are sensitive to nifuroxazide, while *ALDH1A3* loss-of-function mutations confer drug resistance. In tumors, nifuroxazide targets ALDH1^{High} melanoma subpopulations with the subsequent loss of melanoma-initiating cell potential. BRAF and MEK inhibitor therapy increases ALDH1 expression in patient melanomas, and effectively combines with nifuroxazide in melanoma cell models. The selective eradication of ALDH1^{High} cells by nifuroxazide-ALDH1 activation goes beyond current strategies based on inhibiting ALDH1 and provides a rational basis for the nifuroxazide mechanism of action in cancer.

Keywords: melanoma, ALDH, cancer stem cells, tumor-initiating cells, pro-drugs, nifuroxazide, 5-nitrofurans, drug targets, drug mechanism of action, BRAF inhibitor

Graphical Abstract

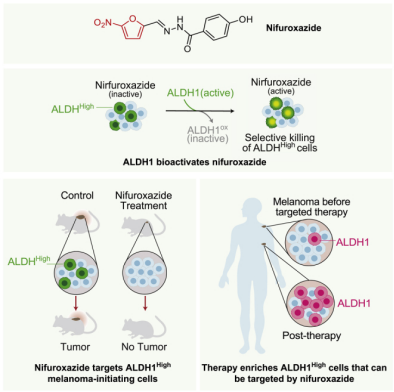

Introduction

5-Nitrofurans are pro-drugs (i.e., they require bio-activation for activity) and have been widely used in human and veterinary medicine for over 40 years to treat bacterial and trypanosome infections (Clayton, 2010). Recently, 5-nitrofuran antibiotics, such as nifurtimox and nifuroxazide, have been found to have anti-cancer activity in cancers, including neuroblastoma, melanoma, multiple myeloma, colon, and breast cancer (Nelson et al., 2008, Saulnier Sholler et al., 2006, Saulnier Sholler et al., 2011, Yang et al., 2015, Ye et al., 2017, Zhou et al., 2012, Zhu et al., 2016). Notably, nifurtimox reduced neuroblastoma tumor burden in a child with Chagas disease caused by trypanosome infection (Saulnier Sholler et al., 2006), and is now in a phase II clinical trial to treat children with relapsed or refractory neuroblastoma or medulloblastoma (NCT00601003) (Saulnier Sholler et al., 2011). When used to treat infectious disease, the relative selectivity of the 5-nitrofurans is mediated by bio-activation by bacterial- or parasite-specific nitroreductases (Clayton, 2010). However, the mechanism by which 5-nitrofurans confer anti-cancer activity is not well understood, limiting efforts for 5-nitrofuran drug development, patient stratification, and the development of treatment strategies.

We previously discovered that aldehyde dehydrogenase 2 (ALDH2) is a direct target for nifurtimox and NFN1 (a tool compound featuring a 5-nitrofuran moiety) by a small-molecule phenotypic screen in

zebrafish (Zhou et al., 2012). ALDH enzymes are a large family of enzymes that metabolize toxic aldehydes (Koppaka et al., 2012, Ma and Allan, 2011). ALDH^{High} activity marks somatic stem cells, and, in many cancers, cells with ALDH^{High} enzymatic activity have enhanced tumorigenic potential and mark so-called cancer stem cell subpopulations (Marcato et al., 2011, Tomita et al., 2016). Cancer cell heterogeneity, including cancer stem cell populations, is of clinical importance because it can make treatment difficult, drive tumor progression, and promote drug resistance (Kreso and Dick, 2014). Genetic and phenotypic cancer cell heterogeneity is especially important in melanoma, where a majority of patients with metastatic melanoma succumb to the disease, and even those who initially respond to targeted or immune treatment may eventually die due to melanoma recurrence and drug resistance (Luke et al., 2017).

Despite the prevalence of the ALDH^{High} subpopulations in multiple cancer types, there are no clinically available drugs that specifically target such subpopulations. Clinically active ALDH inhibitors, such as disulfiram or daidzin, are strong inhibitors for ALDH2, the principal ALDH enzyme responsible for alcohol metabolism, as well as other possible targets (Kona et al., 2011, Koppaka et al., 2012), whereas ALDH^{High} activity in melanoma is mediated by ALDH1A1 and ALDH1A3 (Luo et al., 2012, Yue et al., 2015). Further, ALDH1 inhibitors, although able to reduce enzyme activity, are not designed to eradicate ALDH1^{High} subpopulations (Koppaka et al., 2012, Tomita et al., 2016).

We hypothesized that ALDH1 might bio-activate certain 5-nitrofuran derivatives and thereby eradicate ALDH1^{High} melanoma-initiating subpopulations in tumors. Here, we report that 5-nitrofurans are bio-activated by ALDH1 and show that nifuroxazide, a clinically approved 5-nitrofuran pro-drug, is selectively bio-activated by ALDH1 enzymes over ALDH2 enzymes. This interaction is critical to mediate nifuroxazide anti-tumor activity. Nifuroxazide-induced loss of ALDH1^{High} subpopulations has a direct impact on the melanoma-initiating (cancer stem) cell potential in tumors. This is of clinical importance because we show that BRAF inhibitors lead to an increase in ALDH1^{High} melanoma cells in matched patient biopsies in recurrent metastatic melanoma, and that BRAF inhibitors plus MEK inhibitors lead to an increase in *ALDH1A1* mRNA in matched patient biopsies while on treatment.

Our work argues that an important mechanism of action for nifuroxazide in cancer is through the eradication of ALDH1^{High} cells. These findings lead to two conceptual advances in melanoma therapy that may also be applied more widely to cancer therapy: (1) to selectively kill ALDH1^{High} cell subpopulations, rather than inhibit ALDH1 enzymatic activity, and (2) that the tumor-initiating and stem cell properties of cancer subpopulations can be drug targets, rather than targeting the molecular activity of cancer mutations.

Results

ALDH1 Is a Selective Target for Nifuroxazide

We have previously demonstrated that 5-nitrofuran pro-drugs can be substrates for, and bio-activated by, ALDH2 enzymes, leading to DNA damage and reactive oxygen species to kill cancer cells (Zhou et al., 2012). This prompted us to test if 5-nitrofuran might be bio-activated by ALDH1, yielding an opportunity to specifically target ALDH1^{High} melanoma subpopulations.

To establish the range of concentration of drug activity in cells, we first tested four clinical 5-nitrofurans (nifuroxazide, nitrofurantoin, furazolidone, and nifurtimox), our 5-nitrofuran tool compound NFN1, and the inactive no-nitro control compound NFN1.1 (in which a hydrogen atom replaces the nitro moiety) (Figures 1A, S1A, and S1B). Among the clinical compounds, we found nifuroxazide to have the lowest half

maximal effective concentration (EC_{50}) value in A375 melanoma cell lines and used nifuroxazide as a clinical 5-nitrofuran in our subsequent studies.

Next, we tested the potential for nifuroxazide and NFN1 to be substrates for ALDH1 and ALDH2 enzymes *in vitro*. If 5-nitrofurans are bio-activated by ALDH1, they will compete for ALDH activity toward aldehyde substrates. In this assay, ALDH enzymes metabolize aldehydes and convert NAD+ to NADH. Test substrates that compete for ALDH activity toward aldehydes lead to a reduction in NADH production. As positive controls, we used the ALDH1/2 inhibitor disulfiram, or the potent ALDH2 inhibitor daidzin (Koppaka et al., 2012). We found that both nifuroxazide and the NFN1 tool compound were effective substrates for the ALDH1 isoform ALDH1A3 (Figure 1B), which is highly expressed in melanoma-initiating cell lines.

Surprisingly, while the NFN1 tool compound was a substrate for both ALDH1 and ALDH2 enzymes, nifuroxazide was not an effective substrate for ALDH2 (Figure 1B). These results were validated in a zebrafish ALDH2 activity assay (Figure S1C) (Zhou et al., 2012). Zebrafish melanocytes express ALDH2, and treatment with nifuroxazide (up to 30 μM) did not show any toxicity toward zebrafish melanocytes, whereas treatment with NFN1 (10 μM) significantly reduced the number of melanocytes. To further explore the different selectivity for ALDH2 at equimolar concentrations, we purified ALDH2 and tested its activity with increasing concentrations of NFN1 and nifuroxazide. Dose-curve analysis revealed NFN1 is a highly selective for ALDH2 ($NFN1_{IC50}$ = 63.9 nM), while nifuroxazide had no activity toward ALDH2 up to 10 μM (Figure S1D). Thus, the antibiotic nifuroxazide is a selective substrate for ALDH1.

Next, we used the Aldefluor assay to determine if nifuroxazide might be a substrate of, and modulate, ALDH1 activity in melanoma cells. The Aldefluor assay is based on ALDH enzyme activity to convert the freely diffusible fluorescent BODIPY-aminoacetaldehyde to the negatively charged BODIPY-aminoacetate that is retained and accumulates in the cell. A375 melanoma cell lines are heterogeneous for ALDH activity, with cells presenting low, intermediate, and high fluorescence for Aldefluor activity, which can be seen by fluorescence microscopy (Figure 1C) and used to isolate $ALDH^{High}$ and $ALDH^{Low}$ subpopulations by fluorescence-activated cell sorting (FACS) (Figure 1D). ALDH activity heterogeneity is due, at least in part, to increased mRNA expression of *ALDH1A3* in the $ALDH^{High}$ subpopulation compared with the $ALDH^{Low}$ subpopulation (Figure 1E). Nifuroxazide and NFN1 effectively reduced Aldefluor activity (Figure 1F), indicating that nifuroxazide inhibits ALDH enzyme activity in cells. Inhibition of Aldefluor activity was dependent on the 5-nitro moiety because our no-nitro control compound (NFN1.1) had no effect on ALDH activity in cells (Figure S1E).

To test if 5-nitrofuran activity toward ALDH was linked to the mechanism of melanoma cell death, we tested if N,N-diethylaminobenzaldehyde (DEAB) could prevent 5-nitrofuran cytotoxic activity in cells. DEAB is a potent inhibitor of ALDH1, but also has broad inhibitor activity toward other ALDH enzymes (Koppaka et al., 2012, Luo et al., 2012, Moreb et al., 2012). We found that DEAB pre-treatment protected the cells from the cytotoxicity of NFN1 (Figure 1G). These data indicate that 5-nitrofuran pro-drug cytotoxicity is dependent on ALDH activity.

Nifuroxazide Bio-activation Leads to Oxidation and Inhibition of ALDH1 Enzymes

ALDH1A1 and ALDH1A3 are closely related enzymes and are the predominant ALDH1 isoforms in primary melanoma and melanoma cell lines (Luo et al., 2012). To address the molecular mechanism of how nifuroxazide interacts with ALDH1 enzymes, we first used molecular modeling. The ALDH1A3 structure

has recently been solved (Moretti et al., 2016) and our analysis revealed that nifuroxazide effectively fits into the substrate pocket of ALDH1A3, predicting direct interactions with cysteines 313 and 314 in the active site (Figures 2A and 2B).

To address the potential of 5-nitrofurans to interact with ALDH1A1, we incubated ALDH1A1 with the 5-nitrofurans and performed mass spectrometry of the intact protein (Figure 2C). The results showed ALDH1A1 mass increasing by +35 atomic mass units (amu), consistent with a di-oxidation with nifuroxazide plus NAD+ (42% oxidation of total protein) or NFN1 plus NAD+ (80% oxidation of total protein). In comparison, incubation of ALDH2 with nifuroxazide plus NAD+ did not generate the observed mass shift, while NFN1 plus NAD+ generated both a 31-amu shift and a possible ALDH2-NFN1 adduct (+338 amu) (Figure 2D). The nitro moiety is essential for this process because incubation of NFN1.1 did not generate any additional species with either enzyme (Figures 2C and 2D). Likewise, oxidation of ALDH enzymes by 5-nitrofurans was dependent on NAD+ (Figure S2).

We then used liquid chromatography-tandem mass spectrometry to determine the site of nifuroxazide-catalyzed modification. Quantitative analysis of the modification revealed a significant increase in the oxidation of the catalytic cysteine in the active center of ALDH1A1 upon the addition of nifuroxazide (Figure 2E).

Together, these results demonstrate that nifuroxazide directly and specifically interacts with the ALDH1A1 and ALDH1A3 isoforms leading to oxidation and inactivation of ALDH1 isozymes at the catalytic core. Thus, unlike ALDH1 enzymatic inhibitors, nifuroxazide has a unique two-hit mechanism whereby bio-activation of nifuroxazide by ALDH1 enzymes leads to cytotoxicity concomitant with ALDH1 inactivation (Figure 2F). Nifuroxazide pro-drugs provide an opportunity to move beyond inhibiting ALDH1 enzymes in cancer cells, to selectively eradicating ALDH1-expressing cells in melanoma.

Nifuroxazide Bio-activation Is Mediated by ALDH1A3

Primary melanoma samples express high levels of ALDH1A1 and ALDH1A3, but ALDH1A3 is the predominant form in A375 melanoma cell lines (Luo et al., 2012). If the 5-nitrofuran-ALDH1 interaction is relevant *in vivo*, we would expect that loss of ALDH1 would confer resistance to 5-nitrofuran treatment. Small interfering RNA (siRNA) knockdown of *ALDH1A3* transcripts reduced ALDH1A3 protein levels and Aldefluor activity, and validates ALDH1A3 as the dominant ALDH1 enzyme responsible for Aldefluor activity in melanoma A375 cells (Figures 3A and 3B). Next, we tested the sensitivity of these cells to NFN1, and found siRNA *ALDH1A3* cells to have significantly reduced sensitivity to NFN1 toxicity (Figure 3C).

Further, we generated *ALDH1A3* mutant lines using CRISPR/Cas9, and selected two single-cell clones ($ALDH1A3^{Cpr3}$ and $ALDH1A3^{Cpr21}$) that are predicted to be truncated in the N terminus and showed reduced ALDH1A3 protein expression (Figures 3D and S3A) and Aldefluor activity (Figure 3E). Notably, $ALDH1A3^{Cpr3}$ and $ALDH1A3^{Cpr21}$ cell lines had no apparent growth phenotype in culture, and grew at the same rate as control cells indicating that ALDH1A3 is not essential for cell growth in A375 cell culture (Figure S3B). However, $ALDH1A3^{Cpr3}$ and $ALDH1A3^{Cpr21}$ cells had significantly reduced clonogenic potential in soft agar, an assay that tests the ability of a single-cell clonal growth in a 3D environment (Figure S3C) and were unable to form tumors in xenografts (Figure S3D), consistent with the concept that $ALDH^{High}$ subpopulations have functional tumor-initiating characteristics in melanoma cells. Importantly, we found that $ALDH1A3^{Cpr3}$ and $ALDH1A3^{Cpr21}$ cell lines were resistant to nifuroxazide and NFN1 in cell

growth (2D culture) and colony cultures (3D culture) (Figures 3F–3H and S3E–S3H).

Given that loss of ALDH1A3 made cells resistant to nifuroxazide, we hypothesized that overexpression of *ALDH1* should increase cell sensitivity to nifuroxazide. We overexpressed *ALDH1A3* in A375 and C089 melanoma cells by transient transfection, and found that the cells were more sensitive to nifuroxazide than control cells (Figures 3I–3L).

Thus, our genetic analysis confirms that the cytotoxic activity of nifuroxazide in these melanoma cells is mediated by ALDH1, and not an otherwise unknown target enriched in the $ALDH^{High}$ subpopulation. By extension, and in combination with our *in vitro* assays in Figures 1 and 2, it is likely that nifuroxazide is bio-activated in cancers by other ALDH1 isoforms including ALDH1A1.

Nifuroxazide Selectively Kills $ALDH^{High}$ Subpopulations

Having established that ALDH1 enzymes are targets for nifuroxazide in cells, we wanted to test if nifuroxazide is selectively cytotoxic for $ALDH^{High}$ tumor-initiating (stem cell-like) subpopulations. First, we FACS sorted the top 5% of cells highly expressing ALDH enzyme activity ($ALDH^{High}$ cells) and the bottom 5% of cells with the lowest ALDH enzyme activity ($ALDH^{Low}$ cells) (see Figure 1D). The $ALDH^{High}$ cell population had increased sphere-forming potential, which was further increased following serial passage (Figure S4A) and were more efficient at forming colonies in soft agar (Figure 4A). $ALDH^{High}$ cells also had the potential to differentiate into $ALDH^{Intermediate}$ and $ALDH^{Low}$ cells over time while maintaining an $ALDH^{High}$ population, whereas $ALDH^{Low}$ cells were unable to form $ALDH^{High}$ populations (Figure S4B). In addition, *in vivo*, $ALDH^{High}$ cells were more tumorigenic than the $ALDH^{Low}$ cells (Figure S4C). Together, these data validate that the top 5% of $ALDH^{High}$ cell populations are enriched for phenotypic properties associated with stemness and melanoma tumor-initiating potential.

Having separated the cells into $ALDH^{Low}$ and $ALDH^{High}$ populations, and validated their cellular phenotypes, we then tested soft agar colonies derived from each population to increasing concentrations of nifuroxazide and NFN1 (Figures 4B and S4D). We used lower concentrations of drug treatments for the colony assay because the single cells are grown in anchorage-independent conditions and are treated over 21 days to develop into colonies. $ALDH^{High}$-derived colonies were highly sensitive to nifuroxazide and NFN1. In contrast, colonies generated from $ALDH^{Low}$ cells, while producing fewer colonies overall, were resistant to NFN1 and nifuroxazide treatment.

We tested if the paradigm of $ALDH^{High}$ activity and nifuroxazide sensitivity can be extended to melanoma cell lines representative of different melanoma genetic subtypes. We tested Aldefluor activity and nifuroxazide sensitivity in four additional melanoma cell lines: C089 ($BRAF^{V600E}$), C077 ($NF1^{mut}$), MEWO ($NF1^{mut}$), and C092 (triple wild-type) (Ranzani et al., 2015). Aldefluor activity varied widely among cell lines, independently of genetic subtype (Figures 4C and S4E). We found that cell lines with relatively high median levels of ALDH activity formed colonies and were highly sensitive to nifuroxazide (Figures 4D and S4F). In contrast, cells with relatively low median levels of ALDH activity had very low colony formation potential and were resistant to nifuroxazide (Figures 4D and S4F).

Thus, nifuroxazide has selective activity toward multiple cell lines with overall relatively high ALDH activity, and this is independent of melanoma genetic subtype.

Nifuroxazide Targets $ALDH1^{High}$ Subpopulations in Tumors

Ultimately, we wanted to establish if ALDH^{High} subpopulations are selective targets for nifuroxazide *in vivo* and impact tumor growth. We performed a melanoma xenograft assay with human melanoma cells that express a *tdTomato* transgene (A375-L2T cells) enabling us to isolate melanoma cells following treatment. Once the tumors were established, mice were treated with nifuroxazide or with oil vehicle. Nifuroxazide significantly attenuated tumor growth (>10 tumors) (Figures 5A and 5B). We also tested if nifuroxazide could be effective at lower treatment concentrations, and treated A375 melanoma xenografts with 50 or 150 mg/kg for 13 days. Both drug treatments attenuated tumor growth, and in some mice led to partial melanoma regression suggesting that ALDH^{High} subpopulations may be required to support continued tumor growth (Figure S5A). These data suggest that near-maximal drug absorption or efficacy may already be achieved at 50 mg/kg.

Following treatment, we isolated the tumors and analyzed Aldefluor activity in A375-L2T melanoma cells. Tumors treated with nifuroxazide had reduced numbers of ALDH^{High} cells evaluated by Aldefluor assay, indicating that nifuroxazide can target ALDH^{High} subpopulations directly in the tumor (Figure 5C). Strikingly, immunohistochemistry revealed that ALDH1^{High} cells were absent in tumors treated with nifuroxazide (Figures 5D and 5E), accompanied by increased levels of cleaved caspase-3, an apoptosis marker (Figures 5F and 5G). Therefore, nifuroxazide does not just inhibit ALDH enzyme activity in cells, but specifically eradicates ALDH1^{High} tumor subpopulations.

To assess the phenotypic outcome of targeting ALDH1^{High} tumor-initiating subpopulations, we tested if melanoma cells treated with nifuroxazide could initiate new tumors in serial transplantation (Figure 5H). We removed tumors from mice that had been treated with nifuroxazide or oil vehicle, FACS sorted 10,000 melanoma cells per tumor, and injected these into recipient mice without further treatment. Melanomas from mice that had been treated with the oil vehicle control rapidly grew tumors while, in contrast, melanomas from nifuroxazide-treated tumors were significantly inhibited in forming new tumors (Figure 5I). These results were validated in tumors generated from A375 cells without the tdTomato marker, whereby, due to a lack of fluorescence, melanoma cells were selected by excluding endothelial and immune cells (Figure S5B). Therefore, nifuroxazide effectively inhibits tumor growth *in vivo* by selectively targeting ALDH1^{High} subpopulations directly in the tumor, while surviving ALDH1^{Low} cells lack melanoma initiation potential, and are unable to form new tumors.

Targeted Therapy Increases ALDH^{High} Cells and Sensitivity to Nifuroxazide

Little is known about the clinical importance of ALDH1^{High} subpopulations in human clinical samples that have recurred following BRAF inhibitor (BRAFi) and/or MEK inhibitor (MEKi) treatment. First, we performed immunohistochemistry for ALDH1 isoforms on seven patient melanoma samples before BRAFi treatment and in recurrent melanoma from the same patient. The ALDH1 antibody detects both ALDH1A1 and ALDH1A3 isoforms, and thus detects ALDH1 proteins that mark ALDH1^{High} subpopulations in melanoma (Luo et al., 2012). As shown in Figures 6A–6D, four of the melanomas that relapsed after treatment showed a dramatic increase in the number of ALDH1-positive cells and an increase in ALDH1 expression compared with their matched pre-treatment samples. These observations indicate that ALDH1^{High} subpopulations may play an important role during melanoma relapse for some patients.

Next, we tested the potential for nifuroxazide to synergize with BRAF inhibitors. In cell culture, BRAFi lead to an adaptive increase in the number of cells expressing stemness markers, such as ALDH^{High} 24 hr post-treatment (Figure 6E) (Ravindran Menon et al., 2015). Building on these results, we found that

treatment with BRAFi dramatically increased the sensitivity of A375 melanoma colonies to nifuroxazide (Figure 6F).

BRAF signaling depends on MEK activation, and the combination of BRAFi plus MEKi has improved clinical benefit for patients with BRAF mutant melanoma (Luke et al., 2017). To establish if BRAFi plus MEKi increases ALDH1 levels in melanoma, we analyzed RNA sequencing (RNA-seq) data of a melanoma patient cohort before treatment and 12 ± 5 days into BRAFi plus MEKi combined treatment (European Genome-phenome Archive: S00001000992) (Kwong et al., 2015). Of nine patients, six showed an increase in *ALDH1A1* expression while on BRAFi plus MEKi treatment (Figure 6G). These data indicate that for some patients, BRAFi plus MEKi treatment is associated with an increase in *ALDH1A1* expression.

Next, we sought to address if vemurafenib (BRAFi) plus trametinib (MEKi) treatment could lead to an increase in ALDH activity in cell line models and provide a window of opportunity to synergize with nifuroxazide. We found cell lines varied in response and sensitivity to the combined treatment. A375 cells were highly sensitive to MEKi, and the addition of MEKi (2 nM) inhibited the increase in ALDH activity promoted by the BRAFi. In contrast, low concentrations of BRAFi (50 nM) plus MEKi (0.2 nM) lead to an increase in Aldefluor activity in A375 cells (Figure 6H). In C089 cells, BRAFi (1 μM) alone did not significantly increase *ALDH1* mRNA (Figure S6A), while the addition of MEKi alone, or BRAFi plus MEKi, increased ALDH activity at all MEKi concentrations (0.04–2 nM) and was associated with an increase in mRNA expression of *ALDH1A1* (Figures 6H and S6A). Inhibition of the MAPK pathway with MEKi did not increase $ALDH^{High}$ in D38 $NRAS^{Q61K}$ mutant cells at any concentration (0.04–30 nM) (Figure 6H). These data indicate that BRAFi plus MEKi combined therapy can lead to an adaptive increase in $ALDH^{High}$ subpopulations in a subset of melanoma cell lines, although the underlying drug sensitivities may vary. Ultimately, we tested if the therapy-induced ALDH activity increase primed the cells for sensitivity to nifuroxazide. We found that both A375 and C089 cell lines had increased sensitivity to nifuroxazide treatment when combined with the low doses of BRAFi plus MEKi that increase ALDH activity (Figure 6I). These results strengthen the concept that targeted therapy leads to an adaptive increase in ALDH1 in melanoma and provides an opportunity to treat with nifuroxazide.

Discussion

We discover that ALDH1 is a target for the widely used antibiotic nifuroxazide, and that this mechanism selectively targets $ALDH1^{High}$ cells to inhibit tumor growth and initiation potential.

Our results indicate that higher levels of ALDH1 activity in melanoma are associated with increased sensitivity to nifuroxazide, independent of melanoma genotype. This may permit cancer patient stratification for nifuroxazide responsiveness based on ALDH1 activity. Analysis of TCGA RNA expression across tumors reveals melanoma to be among the cancers with the highest *ALDH1A3* overall expression (Figure S6B) (Cancer Genome Atlas Network, 2015, Cerami et al., 2012, Gao et al., 2013b). Targeting $ALDH1^{High}$ subpopulations may be especially important for the 50% of melanoma patients that do not have BRAF mutations and so far have limited options for targeted therapy (Luke et al., 2017).

The clinical evidence we present here indicates that $ALDH1^{High}$ subpopulations increase from primary tumor to BRAFi-resistant metastatic melanomas in some patients, suggesting that melanoma cells may change their cellular state in response to drug treatments. This is supported by analysis of the RNA-seq dataset from patients that reveals some patient melanomas increase *ALDH1A1* expression while on BRAFi plus MEKi. Further analysis of a published RNA microarray dataset (GEO: GSE35230) (Greger et al.,

2012) of A375 clone 16R6-4 revealed that, despite being resistant to BRAFi plus MEKi, combined treatment led to an increase in *ALDH1A3* mRNA expression, suggesting that resistant cells are still sensitized to therapy, and that *ALDH1* expression may contribute to resistance mechanisms (Figure S6C). This drug-induced increase in ALDH1 protein and mRNA underscores the importance in targeting ALDH1^{High} cells, and suggests that an important therapeutic window may be during or following targeted therapy.

Because ALDH^{High} subpopulations are present in many cancer types, major efforts are underway to generate ALDH1 isoform-specific inhibitors. Given that 19 ALDH enzymes are present in the human genome (including at least 6 within the ALDH1 family) (Koppaka et al., 2012), it is not clear at this stage if specific ALDH1 isoform inhibitors will be sufficient to effectively target ALDH^{High} subpopulations in human cancers, or if other ALDH isoforms might be able to compensate and lead to drug resistance. By contrast, we show that nifuroxazide has a two-hit mechanism, whereby it first inactivates ALDH1 through its bio-activation, and, secondly, the bio-activated species generates cytotoxicity to kill the cell. Therefore, rather than transiently inhibiting ALDH1^{High} activity, nifuroxazide selectively kills ALDH1^{High} subpopulations.

Nifuroxazide has been commonly used to treat intestinal infections such as colitis and diarrhea. Bio-activation of 5-nitrofurans in bacteria and trypanosomes generates reactive nitro metabolites and causes DNA damage. Repurposing nifuroxazide as an anti-cancer drug will require the identification of a therapeutic window that selectively targets ALDH1^{High} cells in cancer without eradicating ALDH1^{High} stem cell populations in somatic tissues. Evidence from clinical use of nifuroxazide indicates that nifuroxazide is generally well tolerated (Begovic et al., 2016, Bouree et al., 1989). Nifuroxazide is administered at 800 mg/day in human patients when used as an antibiotic, while in veterinary medicine, animals are often treated at 50 mg/kg, and higher doses (>200 mg/kg) have been described in animals without side effects (Cagliero, 1976, Gao et al., 2013a). We find nifuroxazide is well tolerated in mice at 50 and 150 mg/kg, with no signs of side effects or weight loss. All drug administrations in our *in vivo* studies are oral, as administered for patients when used as an antibiotic. This is a similar dose range used for nifurtimox, which is used at 800 mg/day for trypanosome infection (albeit for 30–90 days), 150 mg/kg/day for pre-clinical neuroblastoma xenograft studies for 28 days (Saulnier Sholler et al., 2009), and at 30 mg/kg/day for cancer treatment (NCT00601003) (Saulnier Sholler et al., 2011). While we cannot directly compare the pharmacokinetics of nifurtimox with nifuroxazide, our studies suggest that nifuroxazide may be effective at targeting ALDH1^{High} cells in a clinically relevant dose range. Importantly, if the combined BRAFi (plus MEKi) and nifuroxazide drug synergy we observe in cell culture holds true in the clinical setting, this may reveal BRAFi (plus MEKi) and nifuroxazide to be a highly beneficial drug combination and permit lower drug doses with reduced overall drug toxicity.

Despite the evidence for melanoma subpopulations in cancer progression and drug resistance, there is an absence of drugs that specifically target phenotypic tumor-initiating cell populations available in the clinic. Indeed, despite the use of nifurtimox in patients with neuroblastoma and medulloblastoma, the mechanism for the anti-cancer activity is unknown. Given that ALDH1^{High} activity marks functional stem cell properties in neuroblastoma (Flahaut et al., 2016, Hartomo et al., 2015), ALDH1^{High} activity might mediate nifurtimox anti-cancer activity. Alternatively, the high levels of ALDH2 in neuroblastoma may mediate sensitivity to nifurtimox (TARGET, 2018). Nifurtimox side effects include a disulfiram-like reaction to alcohol, suggesting that nifurtimox activity may be preferentially bio-activated by ALDH2. This is consistent with our observations that nifurtimox is a competitive substrate for ALDH2 (Zhou et al., 2012)

and that nifuroxazide is selective for ALDH1. Understanding the mechanism of nifurtimox anti-cancer effects may permit patient stratification protocols based on ALDH^{High} activity in the tumor or ALDH2 patient genotypes.

In summary, we have provided substantial mechanistic insights into how a specific 5-nitrofuran used as an antibiotic can act through ALDH1 to reduce melanoma initiation and progression. We believe that such insights are critical to expand the pipeline of cancer drug discovery as it allows us to rationally reposition existing drugs for therapy. The discovery that ALDH1 is a target for nifuroxazide, and that this enables the specific killing of ALDH1^{High} melanoma cells, goes beyond approaches of reducing the tumorigenic potential of such cells by interfering with their ALDH1 activity, which may be limited and transient. This is an important alternative therapeutic strategy to target phenotypically distinct tumor-initiating populations that contribute to melanoma growth and are marked by ALDH1^{High} activity.

Significance

One of the major challenges for cancer treatment and therapeutic design is intratumor heterogeneity, shaped in part by phenotypically distinct tumor cell subpopulations. In melanoma, and in many other cancers, high levels of ALDH activity (ALDH1^{High}) mark a subpopulation of cells with increased tumor-initiation potential and cancer stem cell properties. Here, we show that ALDH1 is a target for 5-nitrofuran pro-drugs that are widely used to treat bacteria infections, and that have recently been shown to have anti-cancer potential.

We have previously shown that 5-nitrofurans are bio-activated by ALDH2, the enzyme responsible for alcohol metabolism. We now show that the 5-nitrofuran, nifuroxazide, is selective for ALDH1, and that the cytotoxic mechanism of action in melanoma cells is mediated by eradicating ALDH1^{High} subpopulations. This is significant because no clinically available drugs have so far emerged to specifically eradicate ALDH1^{High} subpopulations. We show that ALDH1^{High} subpopulations are enriched in patients with recurrent melanoma following BRAF inhibitor treatment and that *ALDH1A1* mRNA is increased in patient melanomas during BRAF plus MEK inhibitor treatment. We demonstrate that nifuroxazide activity in melanoma cells is via a two-hit mechanism: bio-activation by ALDH1 leads to toxicity in cells, coupled with oxidation and inhibition of ALDH1. Thus, unlike ALDH inhibitors, we discover that bio-activation of 5-nitrofuran pro-drugs can selectively kill ALDH1^{High} cell populations. Targeting subpopulations in melanoma based on the distinctive phenotypic properties of tumor-initiating (stem) cells, rather than targeting the molecular activity of cancer mutations, is an orthogonal therapeutic approach to current targeted and immune therapies.

STAR Methods

Key Resources Table

Contact for Reagent and Resource Sharing

Further information and requests for reagents should be directed to the corresponding author E. Elizabeth Patton (e.patton@igmm.ed.ac.uk).

Experimental Model Details

Chemicals Vemurafenib (LKT labs), Trametinib (Selleckchem), Nifuroxazide (EMD Millipore), NFN1

(Maybridge), and clinical 5-nitrofurans were prepared as 100mM solutions in 100% dimethyl sulfoxide (DMSO). NFN1.1 was generated in house following Zhou et al., 2012. Working solutions were freshly prepared before addition to the cell media.

Cell Lines A375 cells were obtained from America Type Culture Collection (ATCC). To generate A375-L2T cells, A375 cells were transfected with ubiquitin promoter-driven L2T (pFU-L2T) and sorted by flow cytometry every week for 3 weeks. L2T lentivirus vector was kindly given by Dr. Sanjiv S. Gambhir (Stanford University) to M.F. through an MTA. DMEM medium, l-glutamine, penicillin/streptomycin and fetal bovine serum (FBS) were purchased from Life Technologies. Cells were maintained in DMEM medium supplemented with 5μg/mL^{-1} l-glutamine, 1% penicillin/streptomycin and 10% FBS and cultured in a humidified 5% CO_2 incubator at 37°C. C077, C092, C089, and MEWO cells were maintained in RPMI-1640 medium (Life Technologies, Thermo Fisher Scientific) supplemented with 1% penicillin/streptomycin and 10% FBS and cultured in a humidified 5% CO_2 incubator at 37°C. All cell lines are routinely tested for mycoplasma by PCR every three months (date of last test June 20, 2018).

***In Vivo* Animal Studies** Female 6–8 week-old NOD/SCID mice were purchased from Charles River Laboratories. Mice were used for tumor xenograft and drug treatment studies. Mice were housed in individually ventilated cages (IVC) in groups of 5-6 mice per cage. All animal experiments were approved by the University of Edinburgh Animal Welfare and Ethical Review Body (approval PL01-16) and the UK Home Office (PPL 70/8897).

Method Details

Generation of ALDH1A3 Mutant Lines Using CRISPR/Cas9 We used two vector system in which the LentiCas9-Blast vector (Addgene; 52962) contained the human codon-optimized *Streptococcus pyogenes* Cas9-expression cassette and the LentiGuide-Puro (Addgene; 1000000049) contained the gRNA expression cassette. The lentiviral vector was produced by transfection of 293T (ATCC) cells with the lentiviral vector plasmid and packaging plasmids pCMVPAX2 (Addgene; 36052) and VSV-g (Addgene; 14888) with polyethylenimine transfection reagent following manufacturer's instructions. 24 hours post transfection, the medium was replaced with fresh media and the cells were cultured for 48 hours. The lentiviral vector containing supernatant was filtered (0.45μm filter) and A375 cells (1×10^4 cells) were transduced with 2ml of LentiCas9-Blast virus particles in 5ml culture media and 5μg polybrene. Transduced cells were selected with 1ng/ml blasticidin to obtain stable cell line expressing Cas9 (A375-Cas9).

SgRNA sequence was cloned in to LentiGuide-Puro. To this, oligos (100μM) were annealed and phosphorylated in 1× T4 ligation buffer with 1× T4 PNK (New England Biolabs) and were ligated into the BsmB1 site of the LentiGuide-Puro vector. One Shot™ Stbl3TM chemically competent E. coli were transformed by adding 100ng of DNA and heat-shocked for 45 seconds at 42°C. Sample was spread on agar with puromycin plates and incubated for 24 hours and single colonies were selected.

SgRNAs were expressed by a transient transfection of the A375-Cas9 cells with LentiGuide-Puro vector described above. Briefly, 5×10^4 A375-Cas9 cells were plated in a 6 well/plate. After 24 hours A375-Cas9 cells were transfected with ALDH1A3-LentiGuide-Puro using Lipofectamine 3000 (0.3μl/well) (Invitrogen) and P3000™ reagent (0.2μl/well). Medium was changed after 24 h. 48 h later, 0.8 μg/ml puromycin (Sigma) was added into transfected cells. Single-cell clones were isolated for sequencing and positive clones (*ALDH1A3^{Cpr3}, and ALDH1A3^{Cpr21}*) were expanded in culture.

ALDH1A3 Overexpression A375 cells were seeded in 96 well plat at 2.5 × 10 cells/well and incubated for 24 hours. Cells were treated 0.1μg *ALDH1A3* overexpressing vector (ALDH1A3/pCMV6-XL4) (Origene) or pCMV6-XL4 empty vector (control) in Opti-MEM™ media with Lipofectamine 3000 (0.3μl/well) (Invitrogen) and P3000™ reagent (0.2μl/well). Medium was changed after 72 hours.

siRNA Transfection A375 cells were seeded in 96-well plate at a density of 2.5×10^3 cells/well or in 6-well plate at a density of 5×10^4 cells/well and incubated for 24 hours. Cells were then treated with 5pmol ALDH1A3 *siRNA* or scrambled control in Opti-MEM™ media with Lipofectamine RNAiMAX (1.5μl/well) (Invitrogen). Medium was changed after 96 hours.

Flow Cytometry and Aldefluor Assay The aldehyde dehydrogenase (ALDH) enzyme activity was measured using the ALDEFLUOR assay kit (STEMCell Technology) according to the manufacturer's protocol. In brief, cells were incubated with the fluorescent bodipy-aminoacetaldehyde (BAAA) reagent for 30 minutes at 37°C. As a negative control, ALDH enzyme activity was blocked using diemethylamino-benzaldehyde (DEAB). Aldefluor activity was measured using FACS Fortessa (BD Biosciences). For cell sorting, the Aldefluor stained cells were analyzed using the FACS Aria II (BD Biosciences) and the top 5% of cell population with highest ALDH activity ($ALDH^{High}$ cells), detected on the green fluorescence channel (515–545 nm), and the bottom 5% of cells with lowest ALDH activity ($ALDH^{Low}$ cells) were cell sorted. Data were analyzed using FlowJo software program. Dead cells were excluded using Propidium iodide (PI, 13μM, Roche) or 4′,6-Diamidine-2′-phenylindole dihydrochloride (DAPI, 3μM, Sigma-Aldrich).

Cell Viability Assay Cytotoxicity of the 5-nitrofurans on melanoma cell lines was determined using the sulforhodamine-B (SRB) cytotoxicity assay (Sigma-Aldrich). 1000 cells per well were plated in 96-well plates overnight. Cells were then treated either with a vehicle control (DMSO) or increasing concentrations of compounds (1nm - 100μM) for 72 hours. SRB assay was carried out as described previously (Skehan et al., 1990). In brief, cells were fixed with Trichloroacetic acid for 1 hour at room temperature, followed by 0.4% SRB for 30 minutes at room temperature. Plates were then washed and the SRB was dissolved by 10mM Tris buffer and read at 570nm on a microplate reader. Experiments were performed in three independent series and the mean half maximal effective concentration (EC50) was used to compare cytotoxicity.

Cytotoxicity and Apoptosis Assays Using IncuCyte ZOOM Live-Cell Imaging System IncuCyte ZOOM Live-Cell Imaging system (Essen Bioscience) was used for kinetic monitoring of cytotoxicity and apoptotic activity of Nifuroxazide or NFN1 on melanoma cells. 1000 cells/well were seeded in 96 well plate and allowed to attach overnight. Cells were treated with increasing concentrations (1nm - 100μM) of compounds in the presence of Draq7™ (3μM, Abcam) and IncuCyte® NucLight BacMam 3.0 (2% v/v) (Essen Bioscience). Draq7™ stains the nuclei in dead and permeabilized cells and IncuCyte® NucLight BacMam 3.0 enables nuclear labelling of living cells. Plates were scanned and fluorescent and phase-contrast images were acquired in real time every 3 hours from 0 to 72 hours post treatment. Normalized green and red object count per well was quantified at each time point and time-lapse curves were generated by IncuCyte ZOOM software. Ratios of Draq7™level in treated cells compared to vehicle were plotted in Microsoft Excel.

Apoptosis Detection Using Annexin V/PI 10^5 cells were seeded in 6-well plates overnight. Cells were then treated with compounds or vehicle for 48 hours. For detection of apoptotic cells, cells were dissociated with cell dissociation buffer and 500μl of binding buffer was added to each sample followed by 5μg/ml of Annexin V–FITC and 5μg/ml of PI. Samples were gently vortexed and incubated for 15 minutes at room temperature in the dark. Samples were analysed using FACS Fortessa (BD Biosciences).

Colony Formation Assay in Soft Agar 5000 cells were suspended in serum free DMEM media supplemented with 10ng/ml EGF, 10ng/ml FGF, B27 supplement (1x, Thermo Fisher Scientific), 5μg/mL^{-1} l-glutamine, and 0.3% low melting agarose (Sigma-Aldrich) in the presence or absence of compounds. Cells were then layered over a solid base of 0.5% low melting agarose in 35mm plastic dishes. The cultures were incubated at 37°C for 12 days. Colonies (>6 cells) from 10 separate fields were counted using a microscope with a 4X objective.

Sphere Formation Assay and Differentiation Assay 1000 sorted ALDH^{High} and ALDH^{Low} cells were cultured in serum free DMEM media supplemented with 10ng/ml EGF, 10ng/ml FGF, B27 supplement (1x), 5μg/mL^{-1} l-glutamine and then plated in low adhesion round bottom plates (Corning®). Cell proliferation was measured by counting disaggregated single cells using a haemocytometer. Dead cells were excluded by using 0.4% Trypan blue solution (Sigma-Aldrich).

For differentiation assay, cell sorted ALDH^{High} and ALDH^{Low} cells were cultured in serum containing (10% FBS) DMEM media supplemented with 5μg/mL^{-1} l-glutamine, 1% penicillin/streptomycin and cultured in tissue culture plates for 5 days. Differentiation of cells evaluated by Aldefluor assay.

Western Blot Analysis Cells were plated at 100,000 cells/well in 6-well plates and allowed to adhere overnight. Cells were lysed with RIPA lysis buffer (Sigma-Aldrich), supplemented with a complete protease inhibitor (Thermo Fisher Scientific Inc.). Protein concentrations were determined using the Bradford assay (Bio-Rad Laboratories) and 25μg protein per lane was electrophoresed on a 12% SDS-polyacrylamide gel in running buffer (Bio-Rad). Gels were transferred onto nitrocellulose membranes using the semi-dry Turbo Transfer system with Turbo Transfer buffer (Bio-Rad). Membranes were probed using rabbit poly clonal ALDH1A3 (1:1000, Invitrogen), and GAPDH (1:5000, Abcam) followed by goat anti-rabbit IRDye 680- or 800- labelled secondary antibodies (LI-COR Biosciences). Membranes were imaged using an Odyssey infrared scanner (LI-COR Biosciences).

***In Vivo* Studies** The tumorigenicity of ALDH^{High} vs ALDH^{Low} cells was compared by injecting 50 A375 sorted cells suspended in 100μl of HBSS containing 30% matrigel (Corning). Cells were introduced via subcutaneous injection to the right flank of mice. Tumor size was measured twice a week with a calliper.

To evaluate the cytotoxicity of nifuroxazide *in vivo*, NOD/SCID mice were injected with 10,000 A375-L2T cells in 30% matrigel via subcutaneous injections. Once tumors were established, animals were allocated to experimental group randomly so that the average tumor size within the experimental group would be the same. Mice were treated with vehicle or 150mg/kg or 50mg/kg nifuroxazide suspended in sunflower oil via oral gavage each day. For serial transplantation studies, once drug treatment was completed, tumors were removed and digested into single cells. For tumor digestion, tumors were minced with a surgical blade and single cell suspensions were generated by enzymatic digestion with 2mg/ml Collagenase D (Roche) for 1 hour at 37°C with intermittent vortexing, followed by passage through 40μm filters (Fisher Scientific). Red blood cells were lysed using Ammonium chloride solution (STEMCELL technology). Cells were washed twice and A375-L2T cells were cell sorted using FACS Aria. 10,000 sorted A375-L2T cells excised from vehicle treated (DMSO) tumor or nifuroxazide treated tumor was suspended in HBSS containing 30% standard matrigel and injected subcutaneously into 6-8 weeks old NOD/SCOD mice. Tumor growth was measured twice a week using calliper.

Immunohistochemistry Paraffin-embedded tissue samples were first de-paraffinized in xylene and re-hydrated in graded washes of ethanol and water. Samples were boiled in pre-warmed 10mM sodium citrate

(pH 6.0) for 10 minutes, followed by incubation in 3% H_2O_2 for 20 minutes and blocked in DAKO® Protein Block Serum-Free (DAKO Agilent pathology solutions) for 1 hour at room temperature. Samples were incubated with ALDH1A3 (1:10000, invitrogen) overnight at 4°C, followed by HRP-conjugated secondary antibodies (Jackson ImmunoResearch Laboratories). Slides were counterstained with Mayer's hematoxylin for 5 minutes.

Patient samples were strained using Leia Bond-III™instrument using the IHC J protocol with Bond Polymer Refine Red Detection System (Leica Microsystems). Antigen retrieval was performed using ER1 solution (Leica Microsystems) for 20 minutes. Sections were then incubated with ALDH1 at 1:300 (BD Biosciences) for 15 minutes, followed by 20 minutes post-primary AP and 30 minutes incubation with polymer AP. Sections were then incubated with Bond Polymer Refine Red Detection System for 15 minutes and counterstained with hematoxylin for 5 min. Slides were washed three times between each step with either bond wash buffer or water.

ALDH1A3 and ALDH2 *In Vitro* Activity Assay The ALDH1A3 *in vitro* activity assay was conducted using commercially bought ALDH1A3 (Life Technologies), and purified ALDH2-His was synthesized in-house was used for ALDH2 (see below). ALDH (5ug) was pre-incubated at 25°C in 50mM sodium phosphate buffer (pH7.4), 0.4mM NAD^+ and drug (1μM NFN1, NFN1.1; 10μM nifuroxazide) or vehicle (1% DMSO) for 10 minutes. Disulfiram or Daidzin (10μM; ALDH1A3 & ALDH2 respectively) was used as a negative control. The assay was initiated by the addition of 0.4mM acetaldehyde. NADH turnover was measured using NanoDrop™ 2000 UV-Vis spectrophotometer at 340nm (ε = 6.22mM/cm) after 10mins to determine ALDH activity against DMSO. Normalized ANOVA were used for statistics.

ALDH2 Protein Purification and Activity Expression from pTrcHis-TOPO® His-tagged human ALDH2 plasmid was achieved through transformation of the plasmid into BL21* *E. coli* and transduction with 1mM Isopropyl β-D-1-thiogalactopyranoside (IPTG). Proteins were extracted through Constant ONESHOT Cell Disruption lysis and lysates, then centrifuged. ALDH2-His was purified on ÄKTApurifier™ UPC 100, first through the HiTrap IMAC FF 1mL column and then through size exclusion using HiLoad™ 16/600 Superdex™ 200 pg size exclusion. ALDH expression was confirmed by gel chromatography and purified ALDH fractions pooled together.

Purified His-tagged ALDH2 (5μg) was pre-incubated at 25°C in 50mM sodium phosphate buffer (pH7.4), 2.5mM NAD^+ plus logarithmic dilution of 5-nitrofuran (NFN1 or NAZ) or 1% DMSO for 10mins. The assay was initiated by the addition of 2.5mM acetaldehyde. NADH turnover was measured using Spectramax M5 plate reader at 340nm (ε = 6.22 mM^{-1} cm^{-1}) for a total of 30mins to determine ALDH activity. The enzymatic rate (V) and IC_{50} values determined were determined using the initial linear change of absorbance between 60 – 300secs. Daidzin (10μM) was used as a positive control and NFN1.1 (10μM) as a negative control.

In Silico Modeling ALDH1A3 with Nifuroxazide Water molecules and other hetero atoms were removed from the structure of ALDH1A3 (PDB 5FHZ) and the program PDB2PQR 2.1.1 used to assigned position-optimised hydrogen atoms, utilising the additional PropKa algorithm with a pH of 7.4 to predict protonation states. The MGLTools 1.5.6 utility prepare_receptor4.py was used to assign Gasteiger charges to atoms. Hydrogen atoms were assigned to compound structures using OpenBabel 2.4.1, utilising the -p option to predict the protonation states of functional groups at pH 7.4. The MGLTools utility prepare_ligand4.py was used to assign Gasteiger charges and rotatable bonds. Autodock 4.2.6 was used to automatically dock the compounds into the retinoic acid binding pocket of the crystal structure. A grid box that encompassed the

maximum dimensions of the cognate ligand plus 12 Å in each direction was used. The starting translation and orientation of the ligand and the torsion angles of all rotatable bonds were set to random. The Autogrid grid point spacing was set at 0.2 Å. The Autodock parameter file specified 50 Lamarckian genetic algorithm runs, 7,625,700 energy evaluations and a population size of 300.

Mass Spectrometry Analysis To analyze ALDH-5-nitrofuran interactions by mass spectrometry, complexes for analysis were formed from 10.0μM of the ALDH isoenzyme with 100μM compound in 2% (v/v) DMSO (final) with or without 500μM NAD+ and incubated for 1 hour at room temperature in 10mM HEPES, pH7.5. Samples (2μL) were injected using an Agilent 1200SL HPLC with a low rate of 0.3mL/min consisting of 70% H2O and 30% acetonitrile with 0.1% formic acid into an Agilent 6520 quadrupole-time of flight (Q-TOF) mass spectrometer operating in TOF mode. The spectra were extracted and deconvoluted using the software packages MassHunter (B.08.00) and Bioconfirm (B.08.00). The abundance levels of the peaks were calculated on the individual deconvoluted spectra using the Bioconfirm (B.08.00) software package.

To analyze the oxidation of ALDH cysteines by 5-nitrofuran, first all unmodified cysteines were alkylated to prevent oxidation during the processing: cysteines already oxidized would not be alkylated, and instead would cascade towards the triply oxidized cysteine sulfonic acid. Next, ALDH1A1 was digested into peptides, and the modified and unmodified peptides were identified on an Agilent Model 6520 QTOF. Proteins from the *in vitro* reaction were suspended in a digest buffer with a final concentration of 0.8 M Urea, 10mM dithiotreitol and 100mM Tris-HCl pH 7.5. Protein solutions were then incubated for 30 minutes at 50°C. Reduced cysteine residues were alkylated by adding iodoacetamide solution to a final concentration of 50mM and incubated 30 minutes at room temperature, in the dark. Proteins were digested with by adding 0.1μg Trypsin and GluC 0.1μg (Promega) per sample for 16 hours at 37°C. Trypsin activity was inhibited by acidification of samples to a concentration of 1% TFA. Digests were desalted on C18 Stage tips and eluates were analysed by HPLC coupled to a Q-Exactive mass spectrometer as described previously (Turriziani et al., 2014). Peptides and proteins were identified and quantified with the MaxQuant software package (1.5.7.4), and label-free quantification was performed by MaxLFQ (Cox et al., 2014). The search included variable modifications for oxidation (M, C, Y, W), dioxidation of (M,C,W), trioxidation (C), carbamidomethylation (C) and carbamidomethylation+oxidation (C) as variable modifications. The false discovery rate, determined by searching a reverse database, was set at 0.01 for both peptides and proteins. Peptide oxidations were relatively quantified by [PeptideOX]/[Peptides].

Quantification and Statistical Analysis

Graphpad Prism software was used for statistical analyses. Statistical and quantification details of experiments can be found in the figure legends. Data are presented as ±SEM of at least 3 independent experiments. Significance was defined a $p<0.05$ between comparison groups.

Acknowledgments

We are grateful to members of the Patton laboratory, James Amatruda, and Heinz Arnheiter for critical reading of the manuscript and helpful suggestions; Craig Nicol and Connor Warnock for assistance with graphic design and figures; Morwenna Muir for assistance with mouse studies; Nathalie M. Spockeli for assistance with Figures S1B and S1C; Martin Wear and Matthew Nowicki for assistance with protein purification and assay development in Figure S1D, supported by the Edinburgh Protein Production Facility (EPPF) and by the Wellcome Trust Multi-User Equipment Grant 101527/Z/13/Z. The authors are grateful to

Dr. Chris Schmidt and colleagues for establishment of the cell lines, and the ABN Cell Line Bank at the QIMR Berghofer Medical Research Institute for provision of these materials. Y.L. acknowledges funding from Zhejiang University School of Medicine; T.D.H. acknowledges NIH grants R21CA198409 and R01CA214567-01; D.M.-R. acknowledges MERIT Award NIH R37AAA11147; A.U.-B. acknowledges EPSRC EP/N021134/1 for funding; M.F. acknowledges the Veterans Affairs Merit Review Award 5I01BX001228 and NIH/NCI R01CA197919; D.J.A. acknowledges the European Union's Seventh Framework Program FP7/2007–2013/ERC synergy grant agreement no. 319661 COMBATCANCER; Cancer Research UK; the Welcome Trust. L.S. acknowledges NIH grant P50 CA174523-02 SPORE on Skin Cancer to the University of Pennsylvania and the Wistar Institute. V.G.B. acknowledges Cancer Research UK grant C157/A24837. E.E.P. is funded by the Medical Research Council (MC_PC_U127585840), an MRC IGMM Translational Science Award, and the European Research Council (ZF-MEL-CHEMBIO-648489). E.E.P. and L.S. acknowledge funding from the L'Oreal-Melanoma Research Alliance Team Science Award (401181).

Author Contributions

S.S., R.C., and Y.L. designed and performed biological experiments. D.R.H. performed *in silico* modeling. T.D.H., L.Z., and A.v.K. performed mass spectrometry. C.-H.C., D.M.-R., M.R., D.J.A., A.U.-B., N.O.C., V.G.B., and M.F. provided reagents and cells lines, and contributed to experimental direction and design. L.S., W.X., and X.X. collected clinical samples and performed immunohistochemistry. M.E.M. is a clinical NHS pathologist and performed the pathology analysis for Figure 6. E.E.P. conceived, designed, and directed the experiments. E.E.P. wrote the manuscript with assistance from S.S., and with input from all authors.

Declaration of Interests

D.J.A. and M.R. have filed a patent application no. 1704267.2. However, the content of the patent is not related to the current manuscript. M.R. currently works at Artios Pharma and own share options of the company. However, none of the work described in this study is related to, based on or supported by the company. T.D.H. holds significant financial equity in SAJE Pharma. However, none of the work described in this study is related to, based on or supported by the company. D.M.-R. and C.-H.C. are advisor to Foresee Pharmaceuticals, who hold their patents related to ALDH2 activators. However, none of the work described in this study is related to, based on or supported by the company. All other authors declare no competing interests.

Notes

Published: October 4, 2018

Footnotes

Supplemental Information includes six figures and can be found with this article online at https://doi.org/10.1016/j.chembiol.2018.09.005.

Supplemental Information

Document S1. Figures S1–S6:

Document S2. Article plus Supplemental Information:

References

Begovic B., Ahmedtagic S., Calkic L., Vehabovic M., Kovacevic S.B., Catic T., Mehic M. Open clinical trial on using nifuroxazide compared to probiotics in treating acute diarrhoeas in adults. Mater. Sociomed. 2016;28:454–458. [PMCID: PMC5239654] [PubMed: 28144199]

Bouree P., Chaput J.C., Krainik F., Michel H., Trepo C. Double-blind controlled study of the efficacy of nifuroxazide versus placebo in the treatment of acute diarrhea in adults. Gastroenterol. Clin. Biol. 1989;13:469–472. [PubMed: 2666238]

Cagliero G. Marxer SpA; 1976. Method of and Fodder for Rearing White-meat Calves for Slaughter.

Cancer Genome Atlas Network Genomic classification of cutaneous melanoma. Cell. 2015;161:1681–1696. [PMCID: PMC4580370] [PubMed: 26091043]

Cerami E., Gao J., Dogrusoz U., Gross B.E., Sumer S.O., Aksoy B.A., Jacobsen A., Byrne C.J., Heuer M.L., Larsson E. The cBio cancer genomics portal: an open platform for exploring multidimensional cancer genomics data. Cancer Discov. 2012;2:401–404. [PMCID: PMC3956037] [PubMed: 22588877]

Clayton J. Chagas disease: pushing through the pipeline. Nature. 2010;465:S12–S15. [PubMed: 20571548]

Cox J., Hein M.Y., Luber C.A., Paron I., Nagaraj N., Mann M. Accurate proteome-wide label-free quantification by delayed normalization and maximal peptide ratio extraction, termed MaxLFQ. Mol. Cell Proteomics. 2014;13:2513–2526. [PMCID: PMC4159666] [PubMed: 24942700]

Flahaut M., Jauquier N., Chevalier N., Nardou K., Balmas Bourloud K., Joseph J.M., Barras D., Widmann C., Gross N., Renella R. Aldehyde dehydrogenase activity plays a key role in the aggressive phenotype of neuroblastoma. BMC Cancer. 2016;16:781. [PMCID: PMC5057398] [PubMed: 27724856]

Gao F., Zhang Q.D., Zhang Z.H., Yan X.D., Zhang H.C., Wang J.P. Residue depletion of nifuroxazide in broiler chicken. J. Sci. Food Agric. 2013;93:2172–2178. [PubMed: 23339038]

Gao J., Aksoy B.A., Dogrusoz U., Dresdner G., Gross B., Sumer S.O., Sun Y., Jacobsen A., Sinha R., Larsson E. Integrative analysis of complex cancer genomics and clinical profiles using the cBioPortal. Sci. Signal. 2013;6:pl1. [PMCID: PMC4160307] [PubMed: 23550210]

Greger J.G., Eastman S.D., Zhang V., Bleam M.R., Hughes A.M., Smitheman K.N., Dickerson S.H., Laquerre S.G., Liu L., Gilmer T.M. Combinations of BRAF, MEK, and PI3K/mTOR inhibitors overcome acquired resistance to the BRAF inhibitor GSK2118436 dabrafenib, mediated by NRAS or MEK mutations. Mol. Cancer Ther. 2012;11:909–920. [PubMed: 22389471]

Hartomo T.B., Van Huyen Pham T., Yamamoto N., Hirase S., Hasegawa D., Kosaka Y., Matsuo M., Hayakawa A., Takeshima Y., Iijima K. Involvement of aldehyde dehydrogenase 1A2 in the regulation of cancer stem cell properties in neuroblastoma. Int. J. Oncol. 2015;46:1089–1098. [PubMed: 25524880]

Kona F.R., Buac D., M Burger A. Disulfiram, and disulfiram derivatives as novel potential anticancer drugs targeting the ubiquitin-proteasome system in both preclinical and clinical studies. Curr. Cancer Drug Targets. 2011;11:338–346. [PubMed: 21247383]

Koppaka V., Thompson D.C., Chen Y., Ellermann M., Nicolaou K.C., Juvonen R.O., Petersen D., Deitrich R.A., Hurley T.D., Vasiliou V. Aldehyde dehydrogenase inhibitors: a comprehensive review of the pharmacology, mechanism of action, substrate specificity, and clinical application. Pharmacol. Rev. 2012;64:520–539. [PMCID: PMC3400832] [PubMed: 22544865]

Kreso A., Dick J.E. Evolution of the cancer stem cell model. Cell Stem Cell. 2014;14:275–291. [PubMed: 24607403]

Kwong L.N., Boland G.M., Frederick D.T., Helms T.L., Akid A.T., Miller J.P., Jiang S., Cooper Z.A., Song X., Seth S. Co-clinical assessment identifies patterns of BRAF inhibitor resistance in melanoma. J. Clin. Invest. 2015;125:1459–1470. [PMCID: PMC4396463] [PubMed: 25705882]

Lang D., Chen F., Milewski R., Li J., Lu M.M., Epstein J.A. Pax3 is required for enteric ganglia formation and functions with Sox10 to modulate expression of c-ret. J. Clin. Invest. 2000;106:963–971. [PMCID: PMC314346] [PubMed: 11032856]

Luke J.J., Flaherty K.T., Ribas A., Long G.V. Targeted agents and immunotherapies: optimizing outcomes in melanoma. Nat. Rev. Clin. Oncol. 2017;14:463–482. [PubMed: 28374786]

Luo Y., Dallaglio K., Chen Y., Robinson W.A., Robinson S.E., McCarter M.D., Wang J., Gonzalez R., Thompson D.C., Norris D.A. ALDH1A isozymes are markers of human melanoma stem cells and potential therapeutic targets. Stem Cells. 2012;30:2100–2113. [PMCID: PMC3448863] [PubMed: 22887839]

Ma I., Allan A.L. The role of human aldehyde dehydrogenase in normal and cancer stem cells. Stem Cell Rev. 2011;7:292–306. [PubMed: 21103958]

Marcato P., Dean C.A., Giacomantonio C.A., Lee P.W. Aldehyde dehydrogenase: its role as a cancer stem cell marker comes down to the specific isoform. Cell Cycle. 2011;10:1378–1384. [PubMed: 21552008]

Moreb J.S., Ucar D., Han S., Amory J.K., Goldstein A.S., Ostmark B., Chang L.J. The enzymatic activity of human aldehyde dehydrogenases 1A2 and 2 (ALDH1A2 and ALDH2) is detected by Aldefluor, inhibited by diethylaminobenzaldehyde and has significant effects on cell proliferation and drug resistance. Chem. Biol. Interact. 2012;195:52–60. [PMCID: PMC3350780] [PubMed: 22079344]

Moretti A., Li J., Donini S., Sobol R.W., Rizzi M., Garavaglia S. Crystal structure of human aldehyde dehydrogenase 1A3 complexed with NAD(+) and retinoic acid. Sci. Rep. 2016;6:35710. [PMCID: PMC5069622] [PubMed: 27759097]

Nelson E.A., Walker S.R., Kepich A., Gashin L.B., Hideshima T., Ikeda H., Chauhan D., Anderson K.C., Frank D.A. Nifuroxazide inhibits survival of multiple myeloma cells by directly inhibiting STAT3. Blood. 2008;112:5095–5102. [PMCID: PMC2597607] [PubMed: 18824601]

Ranzani M., Alifrangis C., Perna D., Dutton-Regester K., Pritchard A., Wong K., Rashid M., Robles-Espinoza C.D., Hayward N.K., McDermott U. BRAF/NRAS wild-type melanoma, NF1 status and sensitivity to trametinib. Pigment Cell Melanoma Res. 2015;28:117–119. [PMCID: PMC4296225] [PubMed: 25243813]

Ravindran Menon D., Das S., Krepler C., Vultur A., Rinner B., Schauer S., Kashofer K., Wagner K., Zhang G., Bonyadi Rad E. A stress-induced early innate response causes multidrug tolerance in melanoma. Oncogene. 2015;34:4448–4459. [PMCID: PMC4442085] [PubMed: 25417704]

Reya T., Duncan A.W., Ailles L., Domen J., Scherer D.C., Willert K., Hintz L., Nusse R., Weissman I.L. A role for Wnt signalling in self-renewal of haematopoietic stem cells. Nature. 2003;423:409–414. [PubMed: 12717450]

Sanjana N.E., Shalem O., Zhang F. Improved vectors and genome-wide libraries for CRISPR screening. Nat. Methods. 2014;11:783–784. [PMCID: PMC4486245] [PubMed: 25075903]

Saulnier Sholler G.L., Bergendahl G.M., Brard L., Singh A.P., Heath B.W., Bingham P.M., Ashikaga T., Kamen B.A., Homans A.C., Slavik M.A. A phase 1 study of nifurtimox in patients with relapsed/refractory neuroblastoma. J. Pediatr. Hematol. Oncol. 2011;33:25–30. [PubMed: 21063221]

Saulnier Sholler G.L., Brard L., Straub J.A., Dorf L., Illeyne S., Koto K., Kalkunte S., Bosenberg M., Ashikaga T., Nishi R. Nifurtimox induces apoptosis of neuroblastoma cells in vitro and in vivo. J. Pediatr. Hematol. Oncol. 2009;31:187–193. [PMCID: PMC4445366] [PubMed: 19262245]

Saulnier Sholler G.L., Kalkunte S., Greenlaw C., McCarten K., Forman E. Antitumor activity of nifurtimox observed in a patient with neuroblastoma. J. Pediatr. Hematol. Oncol. 2006;28:693–695. [PubMed: 17023833]

Skehan P., Storeng R., Scudiero D., Monks A., McMahon J., Vistica D., Warren J.T., Bokesch H., Kenney S., Boyd M.R. New colorimetric cytotoxicity assay for anticancer-drug screening. J. Natl. Cancer Inst. 1990;82:1107–1112. [PubMed: 2359136]

TARGET (2018), Pediatric Neuroblastoma, http://www.cbioportal.org/study?id=nbl_target_2018_pub.

Tomita H., Tanaka K., Tanaka T., Hara A. Aldehyde dehydrogenase 1A1 in stem cells and cancer. Oncotarget. 2016;7:11018–11032. [PMCID: PMC4905455] [PubMed: 26783961]

Turriziani B., Garcia-Munoz A., Pilkington R., Raso C., Kolch W., von Kriegsheim A. On-beads digestion in conjunction with data-dependent mass spectrometry: a shortcut to quantitative and dynamic interaction proteomics. Biology (Basel) 2014;3:320–332. [PMCID: PMC4085610] [PubMed: 24833512]

Yang F., Hu M., Lei Q., Xia Y., Zhu Y., Song X., Li Y., Jie H., Liu C., Xiong Y. Nifuroxazide induces apoptosis and impairs pulmonary metastasis in breast cancer model. Cell Death Dis. 2015;6:e1701. [PMCID: PMC4385941] [PubMed: 25811798]

Ye T.H., Yang F.F., Zhu Y.X., Li Y.L., Lei Q., Song X.J., Xia Y., Xiong Y., Zhang L.D., Wang N.Y. Inhibition of Stat3 signaling pathway by nifuroxazide improves antitumor immunity and impairs colorectal carcinoma metastasis. Cell Death Dis. 2017;8:e2534. [PMCID: PMC5386364] [PubMed: 28055016]

Yue L., Huang Z.M., Fong S., Leong S., Jakowatz J.G., Charruyer-Reinwald A., Wei M., Ghadially R. Targeting ALDH1 to decrease tumorigenicity, growth and metastasis of human melanoma. Melanoma Res. 2015;25:138–148. [PubMed: 25643237]

Zhou L., Ishizaki H., Spitzer M., Taylor K.L., Temperley N.D., Johnson S.L., Brear P., Gautier P., Zeng Z., Mitchell A. ALDH2 mediates 5-nitrofuran activity in multiple species. Chem. Biol. 2012;19:883–892. [PMCID: PMC3684953] [PubMed: 22840776]

Zhu Y., Ye T., Yu X., Lei Q., Yang F., Xia Y., Song X., Liu L., Deng H., Gao T. Nifuroxazide exerts potent anti-tumor and anti-metastasis activity in melanoma. Sci. Rep. 2016;6:20253. [PMCID: PMC4735744] [PubMed: 26830149]

Figures and Tables

Figure 1

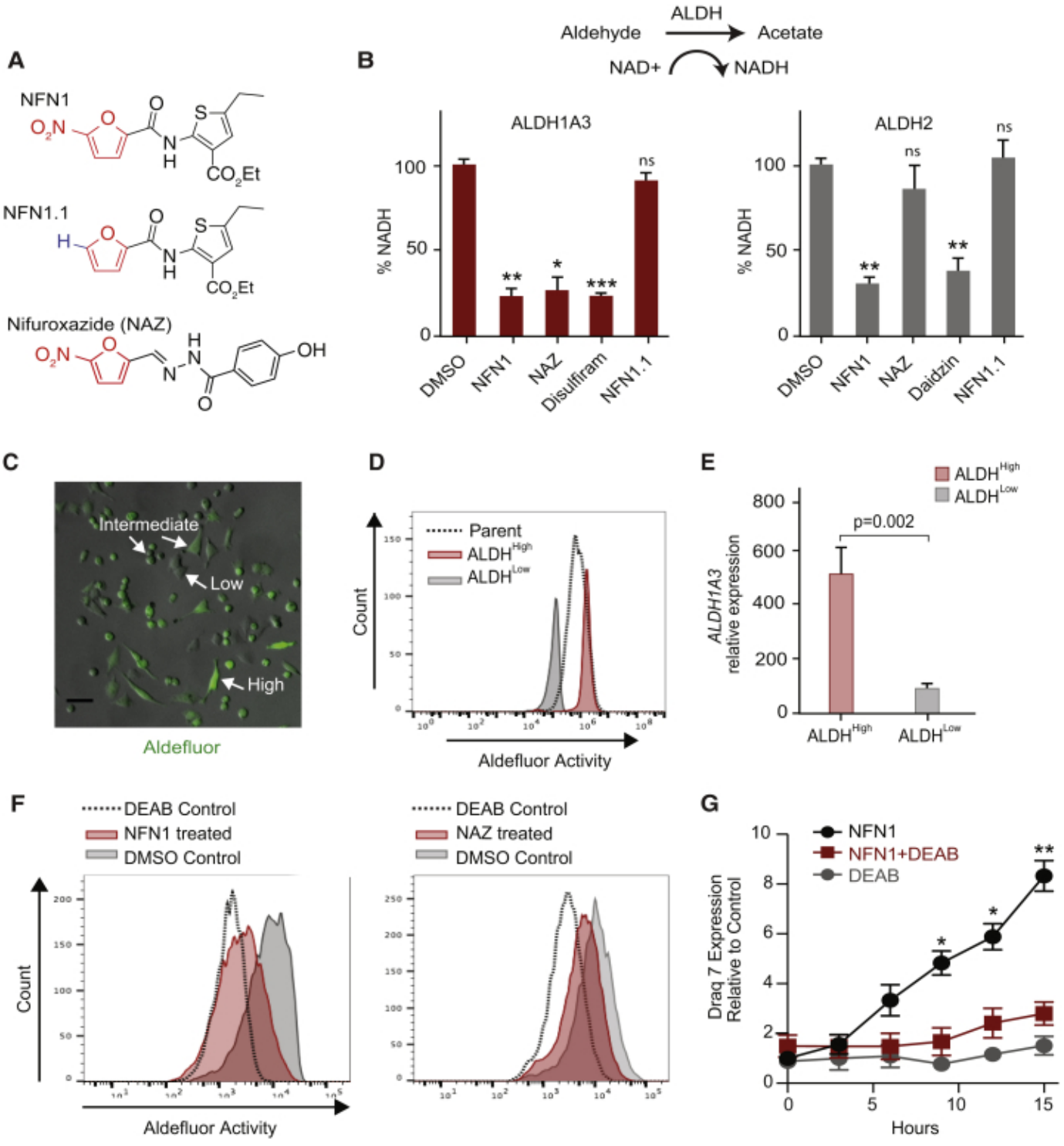

ALDH1 Is a Selective Target for Nifuroxazide

(A) Chemical structures of 5-nitrofuran compounds.

(B) ALDH1A3 and ALDH2 *in vitro* activity assay, with addition of 5-nitrofurans and ALDH inhibitors. Values represent the percent NADH production relative to the DMSO control. Values are means ± SEM (n = 3; *p < 0.05; **p < 0.01; ***p < 0.001, ns, not significant, Student's t test with Dunnett's post-test). Nifuroxazide (NAZ) (10 μM), NFN1 (1 μM),

disulfiram (10 μM), and daidzin (10 μM). Schematic diagram indicates mechanism of NAD+ reduction to NADH by ALDH activity.

(C) Heterogeneity for Aldefluor activity in A375 cells. $ALDH^{High}$, $ALDH^{Low}$, and $ALDH^{Intermediate}$ are indicated (arrows).

(D) Flow cytometry histogram demonstrating Aldefluor activity in A375 unsorted cells and sorted $ALDH^{High}$ and $ALDH^{Low}$ cells.

(E) qRT-PCR for *ALDH1A3* RNA expression in FACS sorted $ALDH^{High}$ and $ALDH^{Low}$ subpopulations. Values are normalized to *GAPDH* RNA expression. Values are means ± SEM (n = 3; Student's t test).

(F) Aldefluor activity in A375 cells treated with 1 μM NFN1, 10 μM nifuroxazide, or DMSO control for 24 hr (n > 3). DEAB used as negative control.

(G) Sensitivity of A375 cells to NFN1 +/− DEAB. Cytotoxicity was evaluated by Draq7 expression using IncuCyte Zoom. Values are means ± SEM (n = 3; *p < 0.05; **p < 0.01, ANOVA with Tukey's test).

See also Figure S1.

Figure 2

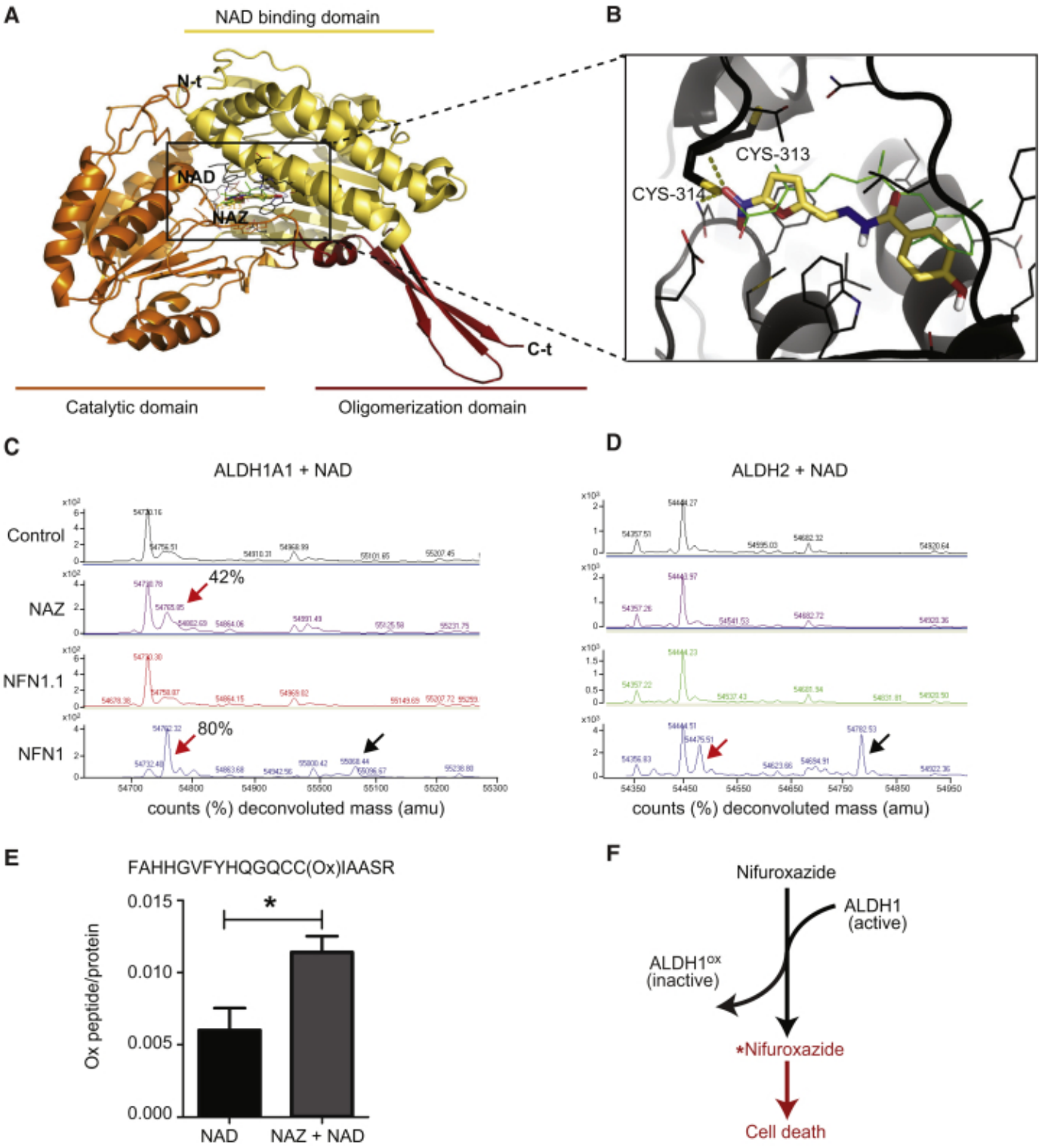

Nifuroxazide Bio-activation Leads to Oxidation and Inhibition of ALDH1 Enzymes

(A and B) Molecular modeling of ALDH1A3 with nifuroxazide (NAZ) and NAD. Nifuroxazide (color filled) forms molecular bonds with the cysteines 313,314 in the active site.

(C and D) Mass spectrometry traces of ALDH1A1 and NAD (C), and ALDH2 and NAD (D) in combination with 5-nitrofurans and control compounds or DMSO. Red arrows indicate oxidized ALDH1A1 and ALDH2 species, black arrows indicate enzyme-5-nitrofuran adducts.

(E) Liquid chromatography-tandem mass spectrometry (LC-MS/MS) quantitative analysis of oxidation of the catalytic cysteines in the active center of ALDH1A1 with nifuroxazide. Values are normalized by dividing the intensity of the

oxidized peptide over the sum of all intensities of all peptides identified in the protein (ratio ox-pep/protein) (*p < 0.05, Student's t test).

(F) Schematic diagram of nifuroxazide two-hit mechanism of action. ALDH1 enzymes bio-activate the nifuroxazide pro-drug, leading to reactive nitro species (*Nifuroxazide) and cell toxicity, and concomitantly oxidize and inactivate ALDH1.

See also Figure S2.

Figure 3

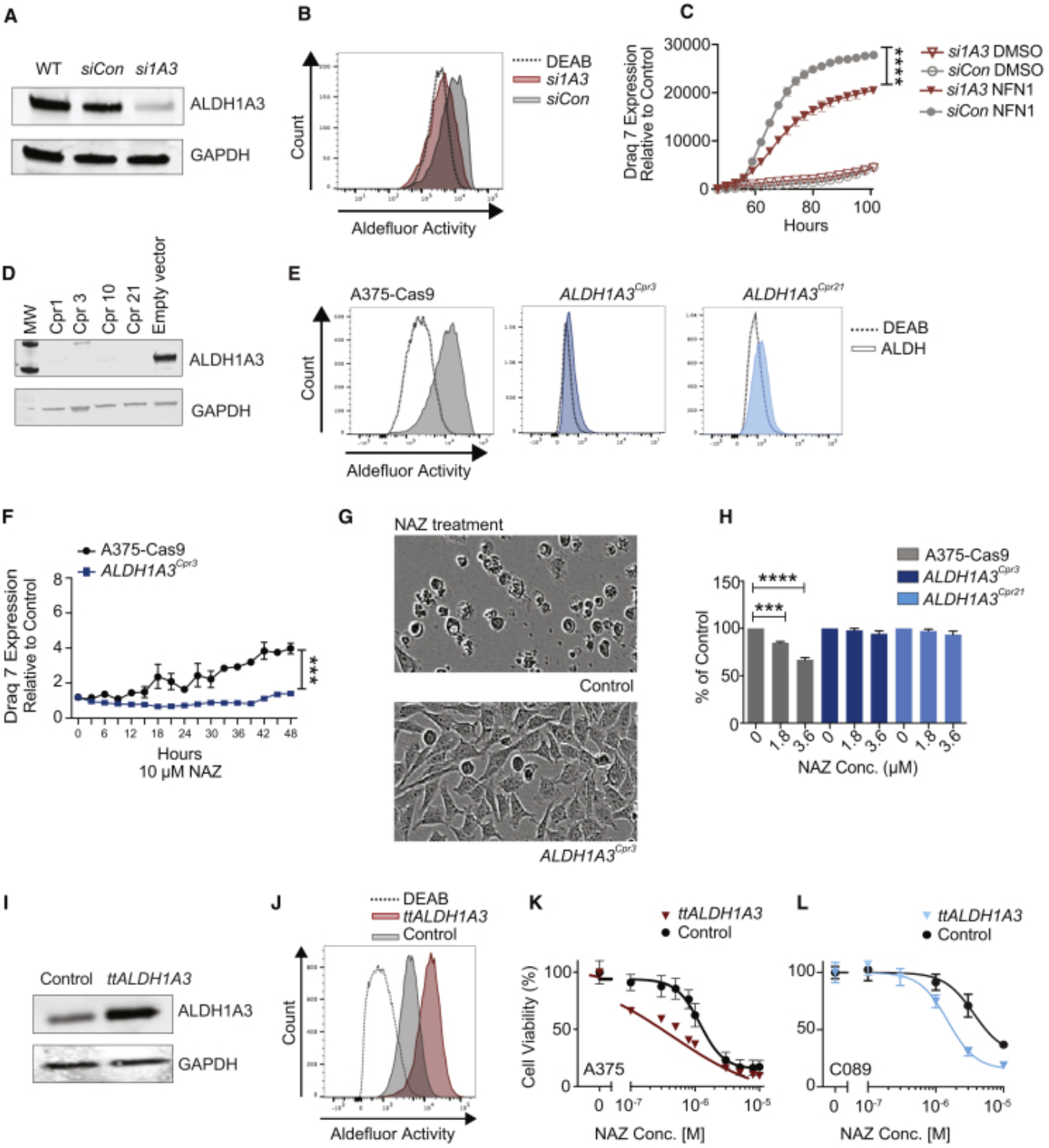

ALDH1A3 Mediates Nifuroxazide Activity

(A) Western blot of ALDH1A3 in *ALDH1A3* siRNA transfected A375 (*si1A3*) cells, siRNA control (*siCon*), and wild-type (WT) control cells. GAPDH, loading control.

(B) Aldefluor activity in *si1A3* cells or *siCon* cells. DEAB was used as a negative control (n > 3).

(C) Sensitivity of *si1A3* and *siCon* cells to NFN1 measured by levels of Draq7 expression using IncuCyte Zoom. Values are means ± SEM (n = 3, ****p < 0.0001, ANOVA with Tukey's test).

(D) Western blot of ALDH1A3 protein in *ALDH1A3* knockout single-cell clones. GAPDH, loading control (n > 3).

(E) Aldefluor activity in *ALDH1A3* knockout clones and A375-Cas9 WT cells. DEAB is used as negative control.

(F) Sensitivity of $ALDH1A3^{Cpr3}$ and A375-Cas9 cells to 10 μM nifuroxazide measured by levels of Draq7 expression using IncuCyte Zoom. Values are means ± SEM (n = 4, ***p < 0.001, ANOVA).

(G) Representative images of WT and $ALDH1A3^{Cpr3}$ cells treated with nifuroxazide or DMSO, imaged with IncuCyte Zoom. Note cell death in upper panel.

(H) Clonogenic potential of $ALDH1A3^{Cpr3}$, $ALDH1A3^{Cpr21}$, and control A375-Cas9 cells in soft agar. Values are means ± SEM (n = 3, ***p < 0.001, ****p < 0.0001, ANOVA with Dunnett's test).

(I) Western blot image of ALDH1A3 protein levels in A375 cells overexpressing *ALDH1A3* (transient transfection *ALDH1A3* [*ttALDH1A3*]) and WT control cells. GAPDH, loading control.

(J) Aldefluor activity in *ttALDH1A3* and WT control. DEAB was used as negative control.

(K and L) Sensitivity of A375 (K) and C089 (L) cells, control and overexpressing *ALDH1A3* to nifuroxazide. Viability was measured using SRB assay. Values are means ± SEM (n = 3).

See also Figure S3.

Figure 4

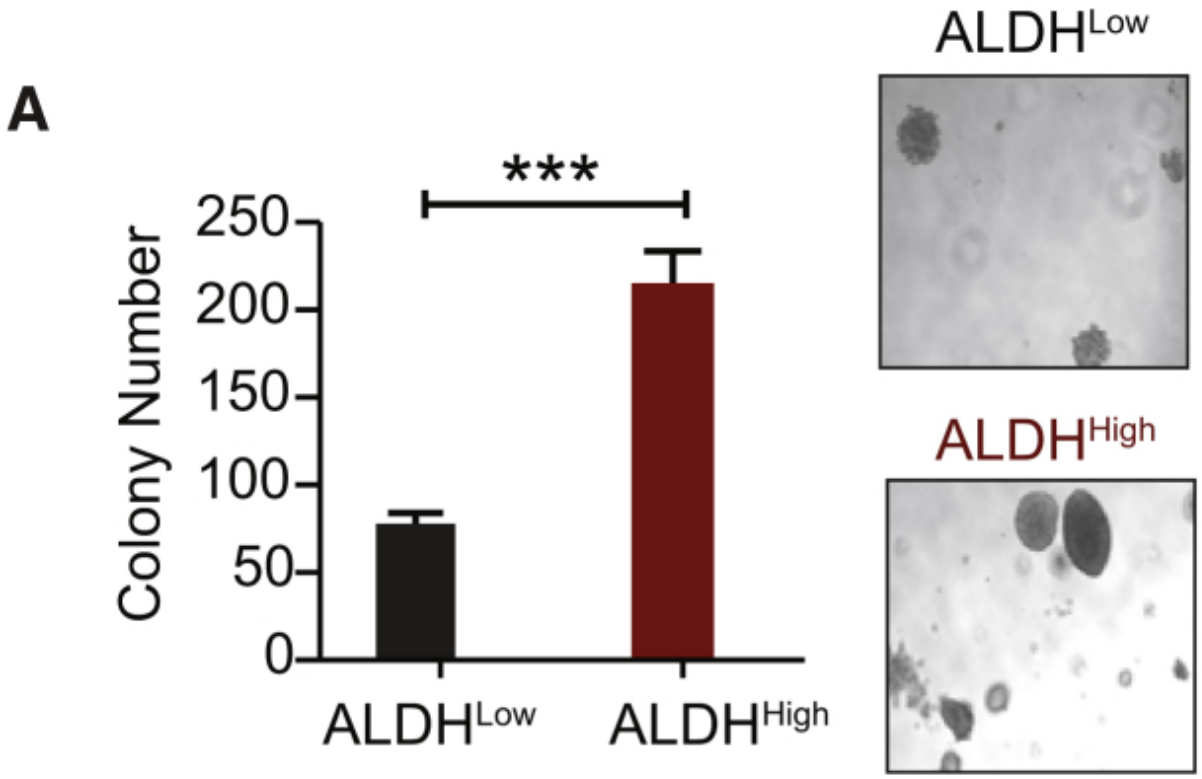

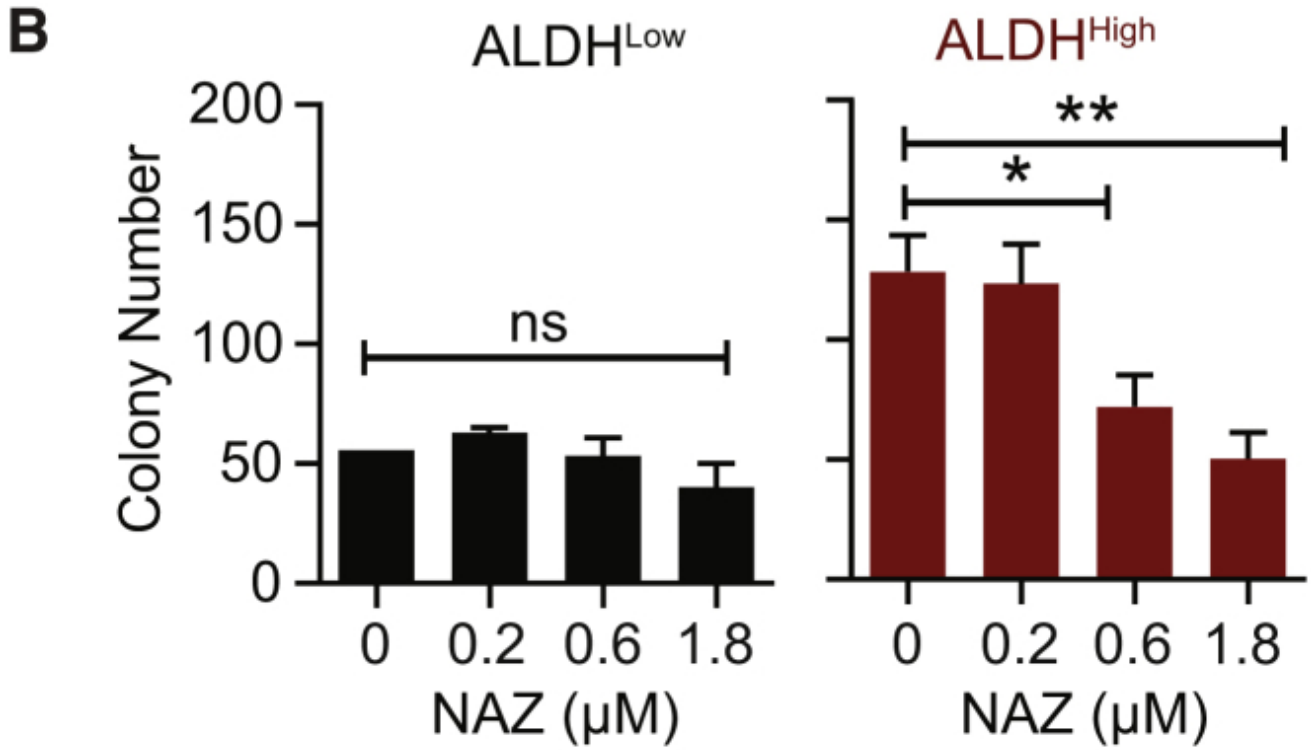

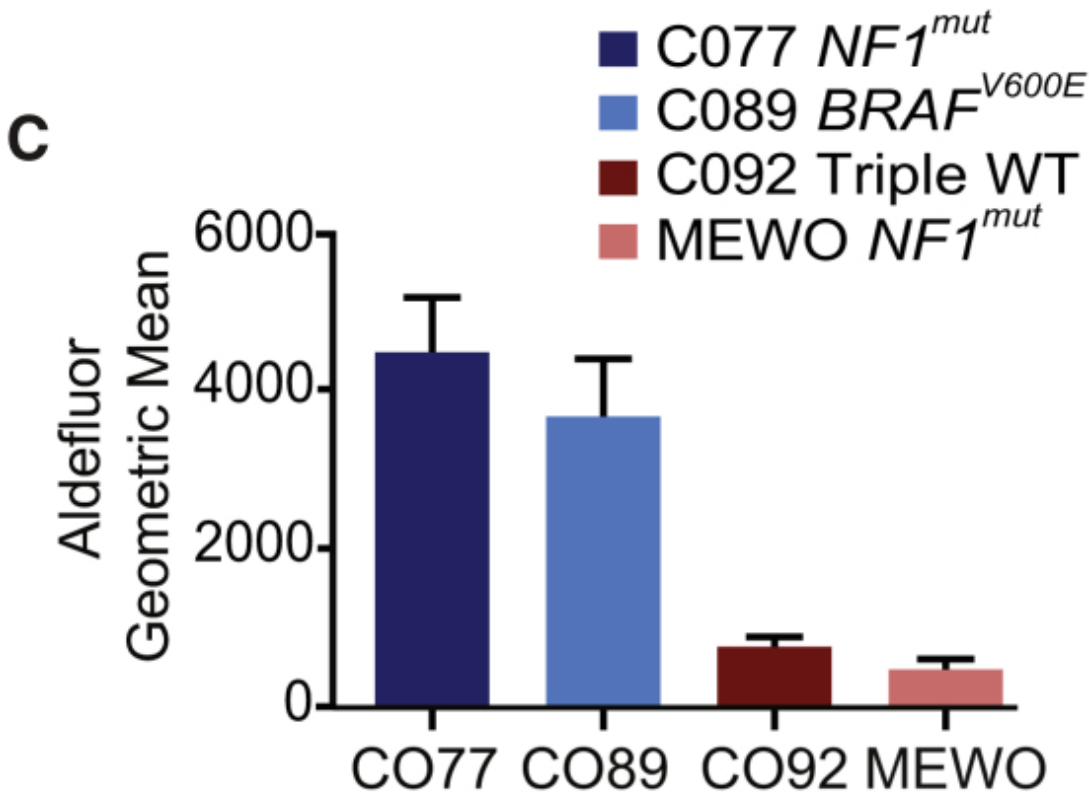

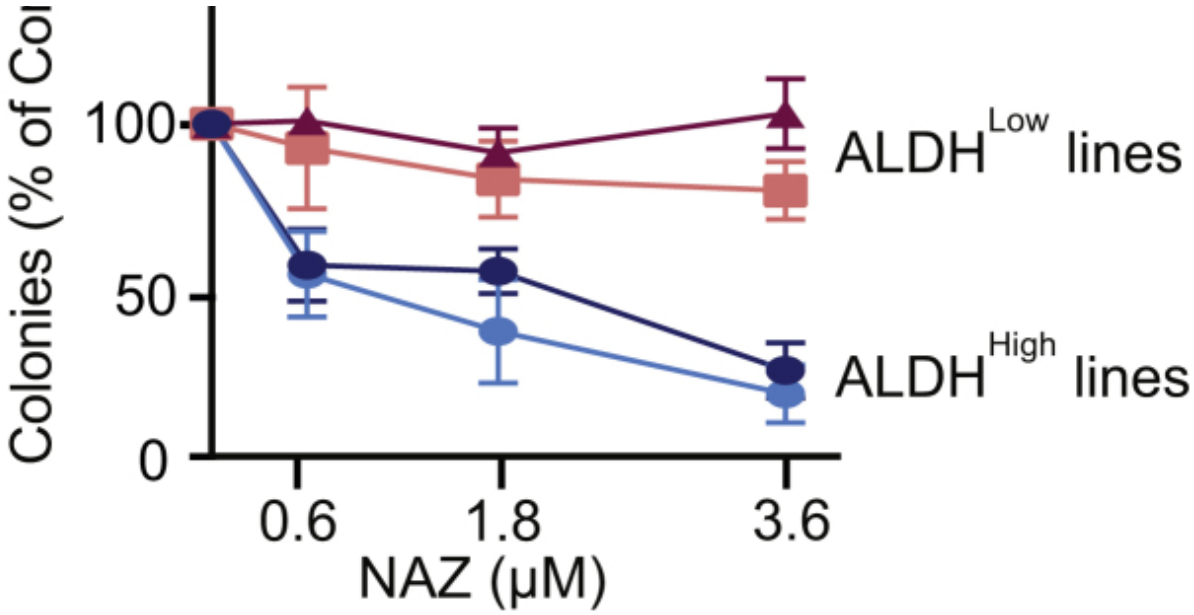

Open in a separate window

ALDH^{High} Melanoma Cells Are Selectively Sensitive to Nifuroxazide

(A) Clonogenic potential of ALDH^{High} and ALDH^{Low} in soft agar. Values are means ± SEM (n = 3; ***p < 0.001. Student's t test). Representative images of colonies formed by ALDH^{High} and ALDH^{Low}.

(B) Sensitivity of ALDH^{High} and ALDH^{Low} colonies to nifuroxazide or DMSO (control). Values are means ± SEM (n = 3; *p < 0.05, **p < 0.01, ns, not significant, ANOVA with Dunnett's test).

(C) Geometric mean of Aldefluor activity in melanoma cells of different genetic subtypes.

(D) Sensitivity of melanoma lines to nifuroxazide as measured by number of colonies in soft agar. Values are means ± SEM (n = 3).

See also Figure S4.

Figure 5

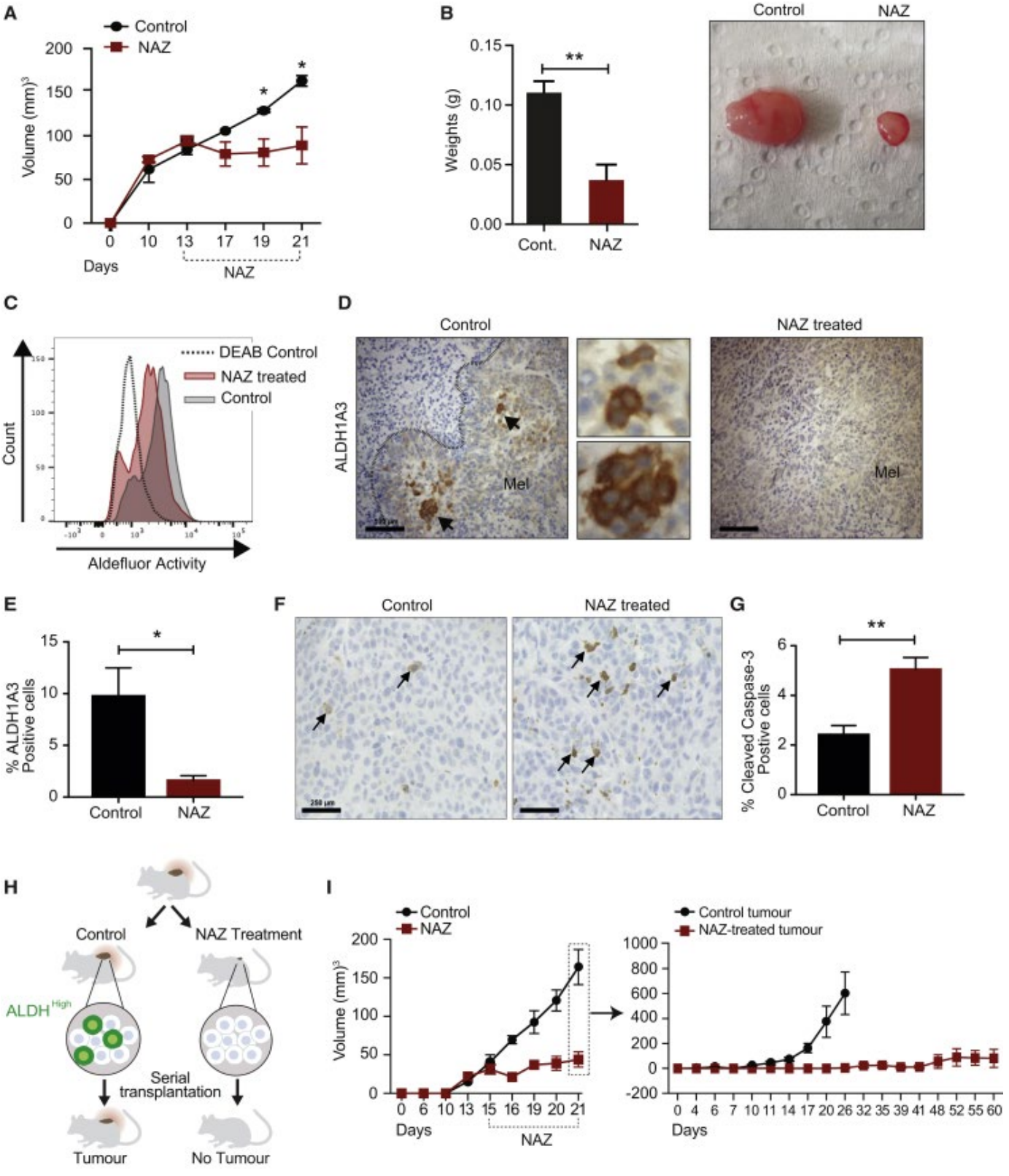

[Open in a separate window](#)

Nifuroxazide Targets ALDH1A3^{High} Subpopulations in Melanoma Tumors

(A) Sensitivity of A375-L2T tumors to nifuroxazide *in vivo*. Mice were treated with 150 mg/kg nifuroxazide or vehicle for 9 continuous days. Values are means ± SEM (n = 3 mice/condition; experimental replicates >3, *p < 0.05, two-way ANOVA with Sidak's test).

(B) Tumor weights of control or nifuroxazide-treated mice at the end of drug treatment. Values are means ± SEM (n = 3

mice/condition; experimental replicates >3, **p < 0.01; Student's t test). Image of tumors from control or nifuroxazide-treated mice at the end of drug treatment duration.

(C) Aldefluor activity in A375-L2T cells in tumors treated with nifuroxazide or vehicle for 9 days. Note the significant shift to the left in the tumors from nifuroxazide-treated mice indicating reduced Aldefluor activity (geometric mean of Aldefluor activity; n = 3 p < 0.05; Student's t test).

(D) Immunohistochemistry staining of ALDH1A3 expression in melanoma tumors generated from A375-L2T cells treated with nifuroxazide or vehicle for 5 days (n = 3). 20×. Scale bar, 100 μm. Arrows point to ALDH1^{High} cell clusters. Mel, melanoma tumor. Dotted lines outline tumor.

(E) Quantification of ALDH1A3-positive cells in melanoma tumors treated with nifuroxazide or vehicle. The percentage mean of ALDH1A3-positive cells in melanoma tumors treated with nifuroxazide or vehicle from 10 random fields of view with 10× magnification is presented (*p < 0.05; Student's t test).

(F and G) Representative image of immunohistochemistry staining, 40×. Scale bar, 50 μm (F) and quantification of cleaved caspase-3-positive cells of melanoma cells in tumors treated with nifuroxazide or vehicle (n = 3) (G). The percentage mean of cleaved caspase-3-positive cells from 10 random fields of view with 10× magnification is presented (**p < 0.01; Student's t test).

(H) Schematic diagram of the experimental outline in (F) for nifuroxazide effect on tumor-initiating potential.

(I) Tumor-initiating potential of nifuroxazide- or control-treated tumors in recipient mice. Mice with established tumors were treated with nifuroxazide or oil for 6 days, tumors were removed and isolated A375-L2T cells were injected into recipient mice without further treatment. Values are means ± SEM (n = 3 mice/condition).

See also Figure S5.

Figure 6

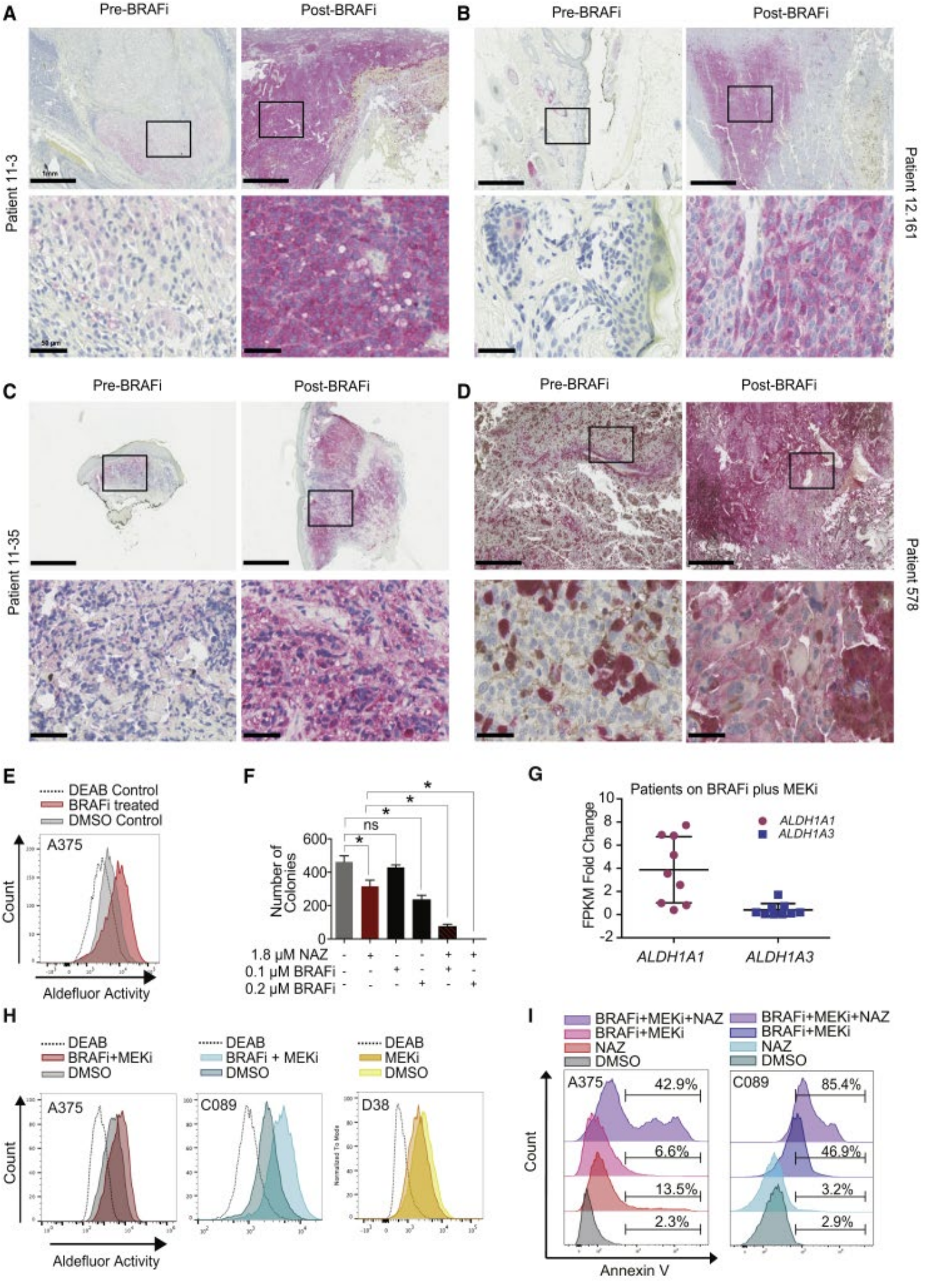

Open in a separate window

ALDH^{High} Cells Are Enriched in Melanoma Patient Samples Following Targeted Therapy

(A–D) Immunohistochemistry of ALDH1 expression in melanoma patient samples. Matched patient samples were taken before and after vemurafenib treatment. Images are shown at 2.5× and 40× magnification. Boxes indicate the region in which the image has been captured with a 40× magnification. Scale bars, 1 mm (2.5×) and 50 μm (40×). The four of seven matched patient samples that showed an increase in ALDH1 post-treatment are presented.

(E) Representative flow cytometry histograms of Aldefluor activity in A375 cells treated with vemurafenib (BRAFi) or DMSO control (n = 2).

(F) Sensitivity of A375 colonies in soft agar to nifuroxazide in combination with BRAFi. Values are means ± SEM (n = 2, *p < 0.05, ANOVA with Dunnett's test).

(G) Pair-matched FPKM fold change of melanoma *ALDH1A1* and *ALDH1A3* in BRAF and MEK inhibitor-treated patient samples on-treatment versus pre-treatment, based on the RNA-seq data retrieved from the European Genome-phenome Archive S00001000992 database. Collective fold-change values are present as means ± SEM. FPKM, fragments per kilobase of transcript per million mapped reads.

(H) Aldefluor activity of melanoma cell lines treated with BRAFi plus trametinib (MEKi), or DMSO control 24 hr post-treatment (n = 3). A375 (50 nM BRAFi + 0.2 nM MEKi), C089 (1 μM BRAFi + 0.04 nM MEKi), or D38 (0.04 nM MEKi).

(I) Representative flow cytometry analysis demonstrating percentage of Annexin V-positive cells. A375 cells treated with 10 μM nifuroxazide, 50 nM BRAFi, and 0.2 nM MEKi for 48 hr (n = 2). C089 treated with 5 μM nifuroxazide, 1 μM BRAFi, or 0.04 nM MEKi for 48 hr (n = 2).

See also Figure S6.

REAGENT or RESOURCE	SOURCE	IDENTIFIER
Antibodies		
Rabbit poly-clonal ALDH1A3 antibody	Invitrogen	Cat#PA5-15000; RRID:AB_2224038
Mouse mono-clonal GAPDH antibody	Abcam	Cat#Ab8245; RRID:AB_2107448
Mouse ALDH1	BD biosciences	Cat#611194; RRID:AB_2224312
Cleaved Caspase-3 (Asp175) (5A1E) Rabbit mAb	Cell Signaling	Cat# 9664; RRID:AB_2070042
Goat anti mouse IRDye® 680 secondary antibody	LI-COR Biosciences	Cat#925-68070; RRID:AB_2651128
Goat anti rabbit IRDye® 800 secondary antibody	LI-COR Biosciences	Cat#925-32211; RRID:AB_2651127
CD271-PE	Miltenyi Biotec	Cat# 130-112-790
FITC anti-mouse CD45 Antibody	BioLegend	Cat# 103107; RRID:AB_312972)
PE anti-mouse H-2K^{b} Antibody	BioLegend	Cat#116507; RRID:AB_313734
APC anti-mouse CD31 Antibody	BioLegend	Cat# 102409; RRID:AB_312904
Bacterial and Virus Strains		

One Shot® Stbl3™ Chemically Competent E. coli	Invitrogen	Cat#C737303
Biological Samples		
Human melanoma tissue	Patient samples were collected by Melanoma Program at the University of Pennsylvania under Institutional Review Board (IRB) approval Protocol #703001 and Abramson Cancer Center's Protocol # UPCC 08607.	
Chemicals, Peptides, and Recombinant Proteins		
Acetic acid	Sigma-Aldrich	Cat#71251
NFN1	Maybridge	Cat#BTB05727SC
Nifuroxazide	EMD Millipore	Cat#481984
Daidzin	Sigma-Aldrich	Cat#30408
Disulfiram	BioVision	Cat#2308
Nitrofurantoin	Sigma-Aldrich	Cat#67-20-9
Nifurtimox	Sigma-Aldrich	Cat#N3415
Furazolidone	Sigma-Aldrich	Cat#F9505
Vemurafenib	LKT-Labs	Cat#029872-54-5
DEAB	STEMCELL technology	Cat#01705
Propidium iodide	Roche	Cat#11348639001
DAPI	Sigma-Aldrich	Cat#D9542
RIPA Lysis buffer (10x)	Sigma-Aldrich	Cat#20-188
Collagenase D	Roche	Cat#11088858001
Ammonium Chloride Solution	STEMCELL Technology	Cat#07850
Annexin V, Alexa Fluor™ 555 conjugate	Thermo Fisher Scientific	Cat#A35108
HEPES	Sigma-Aldrich	Cat#7365-45-9
Cell Dissociation Solution Non-enzymatic	Sigma-Aldrich	Cat#C5914
Complete Protease inhibitor	Thermo Fisher Scientific	Cat#A32953
T4 DNA Ligase	New England Biolabs	Cat#M0202M
T4 DNA Ligase Reaction Buffer	New England Biolabs	Cat#B0202S
Human Recombinant ALDH1A1	Life Technologies	Cat#11388H07E25
Human Recombinant ALDH1A3	Life Technologies	Cat#11636H07E5

Human Recombinant ALDH2	BioVision	Cat#6332
Matrigel Growth Factor Reduced	Corning	Cat#356230
EGF	Thermo Fisher Scientific	Cat#PHG0313
FGF-Basic	R&D	Cat#233-FB-025/CF
B27 Supplement	Thermo Fisher Scientific	Cat#17504044
Low Melting Agarose	Sigma-Aldrich	Cat#A4018
Trametinib	Selleckchem	Cat#S2673

Critical Commercial Assays

Aldefluor Assay	STEMCELL technology	Cat#01705
Cell Meter™ APC-Annexin V Binding Apoptosis Assay Kit	AAT Bioquest®	Cat# 22837
Draq7™	Abcam	Cat#Ab109202
IncuCyte® NucLight BacMam 3.0	Essen Bioscience	Cat#4622
Bond Polymer Refine Red Detection System	Leica Biosystems	Cat#DS9390
Dako REALTM EnVisionTM Detection System, Peroxidase/DAB+, Rabbit/Mouse	DAKO	Cat#K5007
DAKO® Protein block serum-free	DAKO	Cat#X0909
Sulforhodamine B sodium salt (SRB)	Sigma-Aldrich	Cat#S1402
Bradford Assay	Bio-Rad	Cat#500-0006
Lipofectamine® RNAiMAX Transfection Reagent	Invitrogen	Cat#13778150
Lipofectamine® 3000 Transfection Reagent	Invitrogen	Cat#L3000008
Polyethylenimine, Linear, MW 25000, Transfection Grade	Polysciences	Cat#23966-1

Experimental Models: Cell Lines

A375	ATCC	Cat#CRL-1619; RRID:CVCL_0132
293T	ATCC	Cat#CRL-3216; RRID:CVCL_0063
C077	ABN Cell Line Bank, QIMR Berghofer Medical Research Institute	
C089	ABN Cell Line Bank, QIMR Berghofer Medical Research	

	Institute	
C092	ABN Cell Line Bank, QIMR Berghofer Medical Research Institute	
MEWO	ABN Cell Line Bank, QIMR Berghofer Medical Research Institute	
D38	ATCC	
Experimental Models: Organisms/Strains		
Mouse: NOD SCID	Charles River	RRID:IMSR_ARC:NODSCID
Oligonucleotides		
siRNA sequence; Silencer® Select; ALDH1A3, GUAUCGAAGAAGUGAUAAA	Life technology	Cat#4390824
gRNA sequence, ALDH1A3; CACCGCTACATGTAACCCTTCAACT	This paper	N/A
Recombinant DNA		
ALDH1A3 human cDNA clone pCMV6-XL4 vector	Origene	Cat#SC119706
pCMV6-XL4 vector	Origene	Cat#PCMV6XL4
lentiCas9-Blast vector	(Sanjana et al., 2014)	Addgene; 52962
lentiGuide-Puro vector	(Sanjana et al., 2014)	Addgene; 1000000049
pCMVPAX2	(Lang et al., 2000)	Addgene; 36052
VSV.G	(Reya et al., 2003)	Addgene; 14888
Software and Algorithms		
MaxQuant version 1.5.7.4		http://www.coxdocs.orgi
Uniprot Human Proteome, Release 2017_02		http://www.uniprot.org/proteomes/

Open in a separate window